On the effects of exothermicity and endothermicity upon the temperature fields in a partially-filled porous channel

Nader Karimi [1*], Daniel Agbo[1], Ammar Talat Khan[1], Paul L. Younger[1]

[1] School of Engineering, University of Glasgow, Glasgow, United Kingdom

---

Abstract

Forced convection of heat in a two-dimensional channel, partially filled by a porous insert is considered. This system is assumed under fully developed conditions and constant wall heat flux. Further, the fluid and solid phases can feature internal heat generation (exothermicity) and consumption (endothermicity). Analytical solutions are developed for the solid and fluid temperature fields by applying local thermal non-equilibrium (LTNE) conditions and the Darcy-Brinkman model of momentum transport. Two existing interface models (Models A and B) are employed to describe the thermal boundary conditions at the porous-fluid interface. The developed solutions for the temperature fields are compared to those found by applying the local thermal equilibrium (LTE) assumption and, therefore, the validity of the LTE is examined. This is done for a wide range of pertinent parameters including Biot number, conductivity ratio, Darcy number and thickness of the porous insert. It is found that the thermal behaviour of the investigated partially filled system is influenced by the heat sources in both solid and fluid phase. It is further shown that the LTE approach remains an acceptable assumption only for some specific regions of the parametric space. Furthermore, the occurrence of temperature gradient bifurcation on the surface of the porous-fluid interface is examined. It is demonstrated that this effect is highly sensitive to the intensity of the energy sources.

***Key words*:** exothermicity, endothermicity, porous media, porous-fluid interface, local thermal non-equilibrium, temperature gradient bifurcation.

---

1. Introduction

Transport of fluid and heat in porous media continues to attract scientific and technological interest. This is, in part, due to the sustained significance of this topic in classical applications such as energy storage, petroleum engineering, chemical reactors and geothermal energy. In addition, recent advancements in the emerging field of biotechnology has introduced new application areas for heat transfer in porous media [1]. Biological systems mostly involve internal generation of thermal energy in porous media [1,2].There also exist other mechanisms of heat generation in porous media including those through chemical and nuclear reactions, and electrical resistance. Practical examples of these can be found in the storage of agricultural products, chemical reactors, solar and nuclear energy technologies, and electronic cooling. All these systems are temperature sensitive and, therefore, accurate prediction of the temperature fields is an essential part of their thermal analyses. This, in turn, demands a precise approach to the problem of energy transport in these complex, multiphase systems.

There are, fundamentally, two approaches to modelling energy transport in porous media [3-5]. In the first approach, the complex system comprising the solid matrix and the convecting fluid is regarded as a homogenous medium [3,6]. As a result, the fluid and solid phases are assumed to be under local thermal equilibrium (LTE) and thus to have identical temperatures [3,6]. This approach is also referred to as the "one-equation" model. The second approach treats the system as a heterogeneous medium and recognises fluid and solid phases as distinctive phases with different temperatures [7]. Hence, in general it applies a local thermal non-equilibrium (LTNE) condition, and thus includes two energy equations [7]. Expectedly, the latter approach is more realistic and more accurate than the former. However, it requires a significantly more involved analysis and is, therefore, less attractive for practical applications. Hence, it is essential to delineate the validity range of the LTE approach and understand the thermal behaviour of different systems under LTNE conditions. These needs have already motivated a large number of investigations and established an active field of research; see for example [7-11].

Dixon and Cresswell made an early attempt at LTNE modelling of heat transfer in packed beds [12]. Later, Sozen and Vafai considered the transient forced convection of a multi-phase flow through a packed bed and conducted an extensive parametric study [13]. Their analysis included condensation and compressibility effects and employed the LTNE assumption [13]. They reported considerable differences between the solid and fluid temperatures [13]. LTNE analysis was also used to investigate the problem of incompressible flow through a constant temperature channel by Amiri and Vafai [14]. Their analysis showed that increasing both particle Reynolds number and Darcy number favours attainment of LTNE conditions [14]. Application of LTNE analysis to configurations with constant wall heat flux requires an interface model to account for the distribution of heat flux between the fluid and solid phases. The mechanism of splitting heat flux at the interface of a porous medium and an impermeable boundary is not

immediately obvious. As a result, phenomenological arguments are often made to devise interface models. Amiri et al. [8] took this approach and proposed two different interface models. They argued that the wall heat flux boundary condition may be viewed in two different ways [8]. Firstly, a composite system including solid and fluid phases receives the wall heat flux and distributes this between the solid and fluid phases in accordance with their effective conductivities and temperature gradients [8]. Secondly, both solid and fluid phases receive the same heat flux as that of the impermeable boundary [8]. Subsequently, these two basic approaches to interface modelling were respectively regarded as models A and B in the literature [9,15]. Lee and Vafai [15] employed model A and analytically studied the temperature fields and heat transfer characteristics in a fully filled channel subjected to constant heat flux. They studied the physical aspects of heat transfer in porous media and identified a number of regimes in the parametric space [15]. In particular, they highlighted conduction through solid and fluid phases and the subsequent heat exchange between the solid and fluid, as the three basic mechanisms of heat transfer in porous media [15]. They, further, conducted a parametric study on the validity of LTE and showed that decreasing Biot number and fluid to solid conductivity ratio signifies the error associate with the LTE assumption [15].

An extensive study was conducted by Alazmi and Vafai [16] into the influences of variable porosity, thermal dispersion and the LTNE assumption on the heat transfer characteristics of a fully filled channel. They reported that the results of applying the interface models of Amiri et al. [8] could differ from those obtained using the model of Dixon and Cresswell [12], with the degree of agreement depending on the porosity and Reynolds number [16]. The LTNE heat convection analysis was further extended to non-Darcian flow fields by Marafai and Vafai [17]. They used the Darcy-Forchheimer-Brinkman model of momentum transport and developed a set of analytical solutions for the solid and fluid temperature fields. In keeping with Lee and Vafai [15], Marafie and Vafai [17] found that the Biot number and fluid-to-solid conductivity ratios have profound effects upon the validity of the one-equation model. These authors [17] showed that Darcy number and inertial parameter have relatively modest effects on the validity of LTE. A criterion for the validity of LTE was then proposed by Kim and Jang [18]. Through physical scaling analyses these authors argued that LTE dominates as either the interstitial heat transfer coefficient or the interfacial surface area increase [18]. Subsequently, alternative criteria were developed by Jeng et al. [19] for various types of porous media. Khashan and Al-Nimr considered convection of a non-Newtonian fluid through a constant wall temperature, fully filled channel [20]. They argued that LTE mainly depends on Peclet and Biot number and conductivity ratio [20]. Local thermal non-equilibrium analyses were further extended to the developing flows by the numerical analysis of Khashan et al. [21]. They found that LTE

hardly applies to the entrance region of a tube with constant wall temperature and therefore concluded that LTNE should be used for short length tubes [21].

The issue of assigning thermal boundary conditions (interface model) for a constant heat flux problem was highlighted by Alazmi and Vafai [9]. They considered eight different models and incorporated them in a numerical study of the temperature fields and Nusselt numbers [9]. Their extensive parametric study revealed that depending upon the specific problem in hand, models A and B of Amiri et al [8] are the best interface models [9]. Similar to Marafie and Vafai [17], Alazmi and Vafai [9] showed that in a fully filled conduit the effects of inertia parameters upon heat transfer characteristics are rather insignificant. The LTNE analysis and applications of the interface models of A and B were, further, extended to biological applications in a series of analytical works by Mahjoob and Vafai [2,22,23]. Models A and B were then used by Yang and Vafai [24] in their analytical development of the temperature fields and Nusselt number, in a porous filled pipe with internal heat generation. The validity of LTE was investigated in this study under the assumption of Darcian flow and constant wall heat flux [24]. It was shown that heat generating systems can feature temperature gradient bifurcation, in which the fluid and solid temperature gradients on the porous interface have opposite signs [24]. Recently, Ouyang et al. [25] conducted an analytical LTNE study in a thermally developing flow. They showed that the thermal entry length varies with the Biot number, conductivity ratio and the employed interface model.

Application of porous materials in fluid systems is not limited to fully filled conduits and can involve partially filled systems. Partial filling usually reduces the imposed pressure drop, while maintaining most of the heat transfer enhancement characteristics of the fully filled configurations [26,27]. Local thermal equilibrium has been extensively assumed for the heat transfer analysis of partially filled systems (see for example [28-31]). These studies are mainly concerned with the influence of both porous insert configuration and porous media characteristics on the temperature distribution and heat transfer enhancement. Recently, LTNE modelling of partially porous systems has received some attentions. In a numerical study Forooghi et al. [32] found the hydrodynamic field and the Nusselt number in a channel partly filled by a porous insert positioned at the centre of the duct and subjected to constant heat flux. They showed that the change of Nusselt number with porous thickness is not monotonic and can even hinder heat transfer at small thicknesses of the porous insert [32]. Yang and Vafai [33] considered the same configuration as Forooghi et al [32] and analytically solved the Darcy-Forchheimer model under LTNE conditions. They considered a few different porous-fluid interface models and investigated the influences of thermal dispersion and inertia parameter upon temperature fields and heat transfer enhancement [33]. These authors showed that when the condition of equality of temperature gradient at the porous interface is not imposed, heat flux can bifurcate [33]. That is the signs of solid and fluid

temperature gradients on the surface of the porous insert become significantly different. In a separate work Yang and Vafai [34] analysed the validity of local thermal equilibrium in a partially filled channel with constant heat flux walls and under five different interface models. Mahmoudi and Karimi [35] considered a partially filled pipe under constant wall temperature boundary condition. They numerically solved the Darcy-Brinkman- Forshheimer model of fluid flow along with the two-equation energy transport and interface models of A and B [35]. These authors found the optimal porous thickness for enhancement of heat and calculated the induced pressure drops [35]. The corresponding problem in a two-dimensional channel under constant wall heat flux was investigated analytically by Mahmoudi et al. [37] and Karimi et al. [38].

The foregoing review of literature indicates that the comprehensive evaluation of the validity range of LTE in partial porous systems is a substantial task. This is because of the existence of various pertinent parameters and the strong impact of the employed interface model. There have been, so far, a number of attempts for characterisation of thermal behaviour of partially filled systems under LTNE condition [32, 35-38]. Internal heat generation has been ignored in all these studies. On the other hand, it has been already demonstrated that fully filled systems with internal heat generation can feature rich thermal behaviours such as temperature gradient bifurcation [24]. Intuitively, the corresponding problem in partially filled conduits is expected to involve a higher level of complexity. However, there is currently no systematic study of this problem. Given the practical significance of heat generating configurations, this renders itself as an obvious shortcoming. The present work, therefore, aims at addressing this issue through an analytical approach. It builds upon the recent work of Karimi et al. [38] and includes uniform heat generations in both solid and fluid phases.

Figure 1 shows a schematic view of the problem under investigation. Fluid moves into a channel in which a porous material is placed at the core. A constant wall heat-flux boundary condition is imposed on the channel wall. The height of the channel is h_0 and that of the porous material is h_p. Due to the symmetry of the configuration only half of the channel is considered here. Figure 1 is a classical configuration and has been considered previously in other analytical studies [36-38]

In the proceeding analyses, the classical macroscopic theory of transport in porous media [3] is employed and therefore pore scale phenomena are not investigated. The following assumptions are made throughout the current study:

- The porous medium is homogenous and isotropic, fluid saturated and with uniform internal energy generation.
- The flow is laminar, steady and incompressible, with uniform energy generation and no gravity effects.

- Thermally and hydrodynamically fully developed conditions hold in both the open and porous regions.
- It is assumed that Reynolds number is much greater than Grashof number and the emissivity is small. Thus, natural convection and radiation are negligible. It is, further, assumed that viscous heat generation is negligible.
- Physical properties such as porosity, specific heat, density and thermal conductivity are invariants.
- Thermal conductivity is assumed to be constant and therefore thermal dispersion [12,14] effects are ignored here.
- Heat is generated or consumed uniformly and steadily throughout the fluid and solid phases with specified rates.

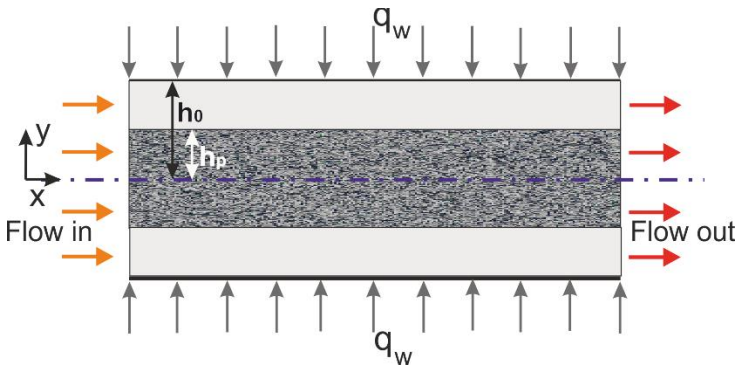

Fig. 1. Schematic of the investigated configuration.

The proceeding analyses and discussions develop the followings. First, closed-form solutions are derived for the temperature fields of the system schematically shown in Fig.1. These exact solutions can be utilised for the validation of numerical studies and other theoretical works. Second, the validity of the local thermal equilibrium assumption in thermal analyses of the system under investigation is examined in section 3. Some selected cases are considered and discussed. Given the analytical nature of this work, those discussions can be readily extended to various other cases. Third, the article aims to develop a physical understanding of the thermal behaviour of the system under investigation (Fig. 1) with interface models A and B and in the presence of internal energy sources. This is important because no superior interface model has been developed to date [16, 17, 37]. Models A and B are generally recognised as the most representative interface models [17, 24]. As a result, the choice of interface model heavily depends upon the physical understanding of the problem under investigation. Detailed analysis of a simple configuration under known conditions, is central to the development of such understanding. This has been previously done for the problems without internal energy sources [37,38]. This paper extends those analyses to an important group of problems, which includes internal exothermicity or endothermicity.

2. Analytical analyses

2.1. Governing equations

Assuming a thermally and hydrodynamically fully developed region, and ignoring free convection and radiative heat transfer, the fundamental equations of heat and fluid flow are reduced to the following forms [36]. The momentum equation in the open region is expressed by:

$$-\frac{\partial p}{\partial x}+\mu\frac{\partial^2 u_f}{\partial y^2}=0. \tag{1}$$

(Terms used in the current analysis are listed in the nomenclature section). The Darcy flow model is limited to the cases in which viscous forces dominate over the inertia forces, such that pore Reynolds numbers remain smaller than unity [7]. Further, it has already been demonstrated that within the porous medium and for $Da\leq 10^{-3}$, the inertia term of the momentum equation is negligibly small [35,39,40]. Thus, in this limit the following Darcy-Brinkman model [7] can be used [35, 37,38]:

$$-\frac{\partial p}{\partial x}+\mu_{eff}\frac{\partial^2 u_p}{\partial y^2}-\frac{\mu}{K}u_p=0. \tag{2}$$

Transport of energy for the open fluid yields:

$$\rho c_p u_f\frac{\partial T_{f1}}{\partial x}=k_f\frac{\partial^2 T_{f1}}{\partial y^2}+S_f. \tag{3}$$

Further, energy balance of the fluid phase in the porous region is:

$$\rho c_p u_p\frac{\partial T_{f2}}{\partial x}=k_{f,eff}\frac{\partial^2 T_{f2}}{\partial y^2}+a_{sf}h_{sf}\left(T_s-T_{f2}\right)+S_f, \tag{4}$$

and the solid phase energy equation can be written as:

$$0=k_{s,eff}\frac{\partial^2 T_s}{\partial y^2}-a_{sf}h_{sf}(T_s-T_{f2})+S_s. \tag{5}$$

2.2. Boundary conditions

The following boundary conditions apply to the momentum equations:

$$u_f=0 \qquad at \quad y=\mathrm{h}_0, \tag{6}$$

$$u_f=u_p,\ \mu_f\frac{\partial u_f}{\partial y}=\mu_{eff}\frac{\partial u_p}{\partial y} \qquad at \quad y=\mathrm{h}_\mathrm{p}, \tag{7}$$

$$\frac{\partial u_p}{\partial y}=0 \qquad at \quad y=0. \tag{8}$$

The energy equations are subjected to the following boundary conditions:

$$\frac{\partial T_{f2}}{\partial y} = \frac{\partial T_s}{\partial y} = 0, \qquad at \qquad y = 0, \tag{9}$$

$$k_f \frac{\partial T_{f1}}{\partial y} = q_w \quad , \quad at \quad y = \mathrm{h}_0, \tag{10}$$

$$T_{f1} = T_{f2}, \qquad at \quad y = \mathrm{h}_\mathrm{p}. \tag{11}$$

Equation (7) express the continuity of the fluid velocity and a balance of shear stress on the porous-fluid interface by using the so called effective viscosity μ_{eff} [36,41,42]. It has previously been shown [43] that setting $\mu_{eff} = \mu_f$ results in acceptable outcomes. The same assumption is, therefore, made throughout this study.

In the present work, two models (model A and B of Yang and Vafai [24] and/or model 1A and model 2A of Alazmi and Vafai [9]) are employed to describe the temperature at the interface between the open and porous regions [37,38]. In model A heat is divided between the two phases on the basis of their effective conductivities and their corresponding temperature gradients [24,37,38] and consequently,

$$q_{\text{interface}} = k_{f,eff} \left.\frac{\partial T_f}{\partial y}\right|_{\text{interface}} + k_{s,eff} \left.\frac{\partial T_s}{\partial y}\right|_{\text{interface}}, \tag{12a}$$

$$\left.T_f\right|_{\text{interface}} = \left.T_s\right|_{\text{interface}} = T_{\text{interface}}. \tag{12b}$$

Model B, on the other hand, assumes that both solid and fluid at the interface receive the same heat flux [24,35,37,38]. That is

$$q_{\text{interface}} = k_{f,eff} \left.\frac{\partial T_f}{\partial y}\right|_{\text{interface}} = k_{s,eff} \left.\frac{\partial T_s}{\partial y}\right|_{\text{interface}}. \tag{13}$$

In Eqs. (12) and (13) $q_{\text{interface}} = k_f \left.\frac{\partial T_{f1}}{\partial y}\right|_{y=\mathrm{h}_\mathrm{p}}$ and $T_{\text{interface}}$ refer to the heat flux and temperature at the porous-fluid interface. By definition, the average flow velocity in the channel is [38]

$$\bar{u} = \frac{1}{\mathrm{h}_0}\left[\int_0^{\mathrm{h}_\mathrm{p}} u_p dy + \int_{\mathrm{h}_\mathrm{p}}^{\mathrm{h}_0} u_f dy\right]. \tag{14}$$

Integrating Eq. (3) from h_p to h_0 and taking into account that in the fully developed region

$\frac{\partial T_{f1}}{\partial x} = \frac{\partial T_{f2}}{\partial x} = \frac{\partial T_f}{\partial x} = \text{const}$, render

$$\rho c_p \frac{\partial T_f}{\partial x}\int_{h_p}^{h_0} u_f dy = (q_w - q_{\text{interface}}) + \int_{h_p}^{h_0} S_f dy. \tag{15}$$

Adding Eqs. (4) and (5) and integrating the sum from 0 to h_p and applying the interface model given by Eq. (12) yield,

$$\rho c_p \frac{\partial T_f}{\partial x}\int_0^{h_p} u_p dy = q_{\text{interface}} + \int_0^{h_p} (S_f + S_s) dy. \tag{16}$$

Further, adding Eq. (15) to Eq. (16) and using Eq. (14) reveal

$$\rho c_p \left.\frac{\partial T_f}{\partial x}\right|_{\text{ModelA}} = \frac{q_w}{h_0}\frac{1}{\bar{u}} + \left(\int_0^{h_0} S_f dy + \int_0^{h_p} S_s dy\right)\frac{1}{h_0 \bar{u}}. \tag{17}$$

By substituting Eq. (17) into Eq. (16) model A prediction of the heat flux at the porous medium-fluid interface can be written as

$$\left.\frac{q_{\text{interface}}}{q_w}\right|_{\text{ModelA}} = \frac{1}{h_0 \bar{u}}\int_0^{h_p} u_p \, dy + \frac{1}{q_w}\left[\frac{1}{h_0 \bar{u}}\left(\int_0^{h_0} S_f dy + \int_0^{h_p} S_s dy\right)\int_0^{h_p} u_p dy - \int_0^{h_p} (S_s + S_f) dy\right]. \tag{18}$$

Adding Eqs. (4) to (5) and integrating the sum from 0 to h_p and applying boundary condition (13) (model B) give the following equation,

$$\rho c_p \frac{\partial T_f}{\partial x}\int_0^{h_p} u_p dy = 2q_{\text{interface}} + \int_0^{h_p} (S_s + S_f) dy. \tag{19}$$

Now, adding Eq. (15) to Eq. (19) and incorporating Eq. (14) yield,

$$\rho c_p \left.\frac{\partial T_f}{\partial x}\right|_{\text{ModelB}} = \frac{1}{h_0 \bar{u}}\left(q_w + q_{\text{interface}}\right) + \frac{1}{\bar{u} h_0}\left(\int_0^{h_0} S_f dy + \int_0^{h_p} S_s dy\right). \tag{20}$$

In a similar way, substituting Eq. (20) into Eq. (19) renders model B prediction of heat flux at the porous medium-fluid interface. This is

$$\left.\frac{q_{\text{interface}}}{q_w}\right|_{\text{ModelB}} = \frac{\int_0^{h_p} u_p \mathrm{d}y}{2h_0 \bar{u} - \int_0^{h_p} u_p \mathrm{d}y} - \frac{\bar{u} h_0}{2\bar{u} h_0 - \int_0^{h_0} u_p dy}\left[\frac{1}{q_w}\int_0^{h_p} (S_s + S_f) dy - \frac{1}{q_w}\frac{\int_0^{h_p} u_p dy}{\bar{u} h_0}\left(\int_0^{h_0} S_f dy + \int_0^{h_p} S_s dy\right)\right]. \tag{21}$$

2.3. Normalisations and velocity profiles

The following dimensionless variables are introduced to normalise the governing equations and boundary conditions.

$$\Theta\big|_{\text{Model A}} = \frac{k_{s,eff}\left(T - T_{\text{interface}}\right)}{q_{\text{w}}\,\text{h}_0}, \tag{22a}$$

$$\Theta\big|_{\text{Model B}} = \frac{k_{s,eff}\left(T - T_{\text{s,interface}}\right)}{q_{\text{w}}\,\text{h}_0}, \tag{22b}$$

$$\gamma = \frac{q_{\text{interface}}}{q_{\text{w}}}, \tag{22c}$$

$$k = \frac{k_{s,eff}}{k_{f,eff}}, \tag{22d}$$

$$Bi = \frac{a_{sf} h_{sf} \text{h}_0^2}{k_{s,eff}}, \tag{22e}$$

$$Y = \frac{y}{\text{h}_0} \tag{22f}$$

$$S = \frac{\text{h}_p}{\text{h}_0} \tag{22g}$$

$$U = \frac{u}{u_r} \tag{22h}$$

$$\omega_f = \frac{S_f \text{h}_0}{q_w} \tag{22i}$$

$$\omega_s = \frac{S_s \text{h}_0}{q_w} \tag{22j}$$

in which u_r is a characteristic velocity defined as $u_r = -\frac{\text{h}_0^{\,2}}{\mu}\frac{\partial p}{\partial x}$ [37,38]. Further, *Bi* is the Biot number, which represents the ratio of the solid phase conduction resistance to the heat exchanged between the fluid and solid phase. It should be noted that the definition of non-dimensional temperatures in Eq. (22a) and (22b), [36-38] leads to the numerical values which are not limited to 0 and 1 and can be negative. It has been already shown that the solutions for Eqs. (1) and (2) and their corresponding boundary conditions (6), (7), and (8) are as follows [36,44]. In the open region,

$$U_f(Y) = -\frac{1}{2}Y^2 + AY + B, \tag{23}$$

$$A = S + \frac{Z\sinh(ZS)(S - 0.5\cdot(1+S^2) + Da)}{Z(S-1)\sinh(ZS) - \cosh(ZS)}, \tag{24}$$

$$B = 1/2 - S - \frac{Z\sinh(ZS)(S - 0.5\cdot(1+S^2) + Da)}{Z(S-1)\sinh(ZS) - \cosh(ZS)}. \tag{25}$$

Within the porous insert,

$$U_p = C\cosh(ZY) + Da\ , \tag{26}$$

$$C = \frac{1}{Z\sinh(ZS)} \cdot (A - S). \tag{27}$$

Considering Eqs. (23) and (26) and the non-dimensional parameters listed in (22), the dimensionless average velocity presented in Eq. (14) reduces to

$$\overline{U} = SDa + \frac{C}{Z}\sinh(ZS) - \frac{1}{6}(1-S^3) + \frac{1}{2}A(1-S^2) + B(1-S), \tag{28}$$

in which, $Z = \sqrt{1/Da}$, S is the ratio of the porous medium thickness to the channel height (Eq. (22g)) and A, B and C have been defined by Eqs. (24), (25) and (27). These velocity fields are then utilised in the solution of the heat flux at the porous-fluid interface and the energy equations. The non-dimensional form of Eq. (18) provides an expression for the heat flux at the porous medium-fluid interface under model A. This is,

$$\gamma\big|_{\text{ModelA}} = \frac{1}{\overline{U}}\int_0^S U_p\, dY + \left[\frac{1}{\overline{u}}\left(\int_0^1 \omega_f\, dY + \int_0^S \omega_s dY\right)\int_0^S U_p\, dY - \int_0^S (\omega_f + \omega_s) dY\right]. \tag{29}$$

Combining Eqs. (26) and (28) gives:

$$\gamma\big|_{\text{ModelA}} = \frac{\frac{C}{Z}\sinh(Z\cdot S) + S\cdot Da}{S\cdot Da + \frac{C}{Z}\sinh(Z\cdot S) - \frac{1}{6}(1-S^3) + \frac{1}{2}A(1-S^2) + B(1-S)} + \left[(\omega_f + S\omega_s)\frac{\frac{C}{Z}\sinh(ZS) + S\cdot Da}{S\cdot Da + \frac{C}{Z}\sinh(Z\cdot S) - \frac{1}{6}(1-S^3) + \frac{1}{2}A(1-S^2) + B(1-S)} - (\omega_s + \omega_f)S\right]. \tag{30}$$

Following the same procedure used in the derivation of Eq. (29), the non-dimensional form of Eq. (21) can be used to derive a relation for the heat flux on the porous-fluid interface under model B. This yields,

$$\gamma\big|_{\text{ModelB}} = \frac{\int_0^S U_p\, dY}{2\overline{U} - \int_0^S U_p\, dY} - \frac{\overline{u}}{2\overline{u} - \int_0^S u_p dY}\left[\int_0^S (\omega_f + \omega_s) dY - \frac{\int_0^S u_p dY}{\overline{u}}\left(\int_0^1 \omega_f\, dY + \int_0^S \omega_s dY\right)\right]. \tag{31}$$

By substituting from Eqs. (26) into (28), Eq. (31) expands to:

$$\gamma\big|_{\text{Model B}} = \frac{\frac{C}{Z}\sinh(ZS)+SDa}{2(SDa+\frac{C}{Z}\sinh(ZS)-\frac{1}{6}(1-S^3)+\frac{1}{2}A(1-S^2)+B(1-S))-\frac{C}{Z}\sinh(ZS)+SDa} -$$
$$\frac{S.Da+\frac{C}{Z}\sinh(ZS)-\frac{1}{6}(1-S^3)+\frac{1}{2}A(1-S^2)+B(1-S)}{SDa+\frac{C}{Z}\sinh(ZS)-\frac{1}{3}(1-S^3)+\frac{1}{2}A(1-S^2)+2B(1-S)}\times \tag{32}$$
$$\left[(\omega_s+\omega_f)S-\frac{\frac{C}{Z}\sinh(ZS)+SDa}{SDa+\frac{C}{Z}\sinh(ZS)-\frac{1}{6}(1-S^3)+\frac{1}{2}A(1-S^2)+B(1-S)}(S\omega_s+\omega_f)\right].$$

2.4 Solid and fluid temperature fields

2.4.1. Model A predictions of the temperature fields

The energy transport equations and the corresponding boundary conditions are derived by substitution of Eq. (22a) into Eqs. (3), (4) and (5). Through this procedure, the energy equation for the fluid in the open region becomes

$$\varepsilon k\frac{U_f}{\overline{U}}(1+\omega_f+S\omega_s)=\Theta''_{f1}(Y)+\omega_f. \tag{33}$$

Transport of energy for the fluid phase within the porous region is written as

$$\frac{U_p}{\overline{U}}(1+\omega_f+S\omega_s)=\frac{1}{k}\Theta''_{f2}(Y)+Bi\left(\Theta_s(Y)-\Theta_{f2}(Y)\right)+\omega_f, \tag{34}$$

and the transport of energy in the solid phase reduces to

$$0=\Theta''_s(Y)-Bi(\Theta_s(Y)-\Theta_{f2}(Y))+\omega_s. \tag{35}$$

The associated energy boundary conditions are as follows,

$$\Theta'_{f1}(1)=\varepsilon k, \tag{36}$$

$$\Theta_{f1}(S)=\Theta_{f2}(S)=\Theta_s(S)=0, \tag{37a}$$

$$\Theta'_{f2}(0)=\Theta'_s(0)=0. \tag{37b}$$

Through, taking the second derivative with respect to *Y*, the two coupled differential Eqs. (34) and (35) are turned into a new set of fourth order ordinary differential equations. These are:

$$\Theta''''_{f2}(Y)-Bi(1+k)\Theta''_{f2}(Y)=\frac{k}{\overline{U}}[-BiU_p(Y)(1+\omega_f+S\omega_s)+U''_p(Y)(1+S\omega_s+\omega_f)]+Bi\cdot k\cdot(\omega_f+\omega_s), \tag{38}$$

$$\Theta''_s(Y)-Bi(1+k)\Theta''_s(Y)=-\frac{k}{\overline{U}}BiU_p(Y)(1+S\omega_s+\omega_f)+Bi\cdot k\cdot(\omega_f+\omega_s). \tag{39}$$

Evaluation of the second and third derivatives of Θ_s and Θ_{f2} at Y=0 and Y=S through substitution of Eqs. (37a) and (37b) into Eqs. (34) and (35) results in,

$$\Theta''_{f2}(S) = k\frac{U_p(S)}{\overline{U}}(1+S\omega_s+\omega_f)-k\omega_f, \qquad \Theta''_s(S) = -\omega_s, \qquad \Theta'''_{f2}(0)=0, \qquad \Theta''_s(0)=0. \tag{40}$$

By integration of the ordinary differential Eq. (33), the following expression is obtained for the temperature distribution of the flow in the open region

$$\Theta_{f1}(Y)\Big|_{\text{ModelA}} = \frac{\varepsilon k}{\overline{U}}\left[\begin{array}{l}(1+\omega_f+S\omega_s)(-\frac{Y^4}{24}+A\frac{Y^3}{6}+B\frac{Y^2}{2})+(1+\omega_f+S\omega_s)(\frac{1}{6}-\frac{A}{2}-B)Y \\ -(1+\omega_f+S\omega_s)(\frac{-S^4}{24}+A\frac{S^3}{6}+B\frac{S^2}{2})+S(1+\omega_f+S\omega_s)\left[-\frac{1}{6}+\frac{A}{2}+B\right] \\ +\overline{U}(Y-S)+\omega_f\frac{\overline{U}}{\varepsilon k}[(Y-S)-\frac{1}{2}(Y^2-S^2)]\end{array}\right], \tag{41}$$

in which A and B are provided by Eqs. (24) and (25). The analytical solution for the temperature distributions in the porous region are developed by solving the differential Eqs. (38) and (39) using the boundary conditions given by Eqs. (37) and (40). This results in the following expressions for the temperature distributions of the fluid and solid phases inside the porous region

$$\Theta_{f2}(Y)\Big|_{\text{ModelA}} = \frac{k}{\overline{U}}\left\{\begin{array}{l}\dfrac{C(Z^2-Bi)(1+S\omega_s+\omega_f)\times[\cosh(ZY)-\cosh(ZS)\times(1+\xi\times Z^2)]}{Z^2(-\Gamma^2+Z^2)} \\ +\dfrac{Bi(Da(1+\omega_f+S\omega_s)-\overline{U}(\omega_f+\omega_s))}{\Gamma^2}\times\left(-\xi+\dfrac{Y^2}{2}-\dfrac{S^2}{2}\right)+ \\ U_p(S)(1+S\omega_s+\omega_f)\xi-\overline{U}\omega_f\xi\end{array}\right\}, \tag{42}$$

$$\Theta_s(Y)\Big|_{\text{ModelA}} = -Bi\frac{k}{\overline{U}}\left\{\begin{array}{l}\dfrac{C(1+S\omega_s+\omega_f)[\cosh(ZY)-\cosh(ZS)\times(1+\xi\times Z^2)]}{Z^2(-\Gamma^2+Z^2)} \\ -\dfrac{Da}{\Gamma^2}(1+S\omega_s+\omega_f)\left(-\xi+\dfrac{Y^2}{2}-\dfrac{S^2}{2}\right)+\dfrac{(\omega_s+\omega_f)\overline{U}}{\Gamma^2}\left(-\xi+\dfrac{Y^2}{2}-\dfrac{S^2}{2}\right)\end{array}\right\}-\omega_s\xi, \tag{43}$$

where $\Gamma=\sqrt{Bi(1+k)}$ and $\xi=\left(\dfrac{\cosh(\Gamma Y)}{\cosh(\Gamma S)}-1\right)\Big/\Gamma^2$.

2.4.2. Model B predictions of the temperature field

Substitution of Eq. (22b) into Eqs. (3), (4) and (5) yields the different forms of the energy transport equation applied to the fluid and solid phases. Transport of energy for the fluid in the open region reduces to

$$\frac{U_f}{\overline{U}}(1+\gamma+\omega_f+S\omega_s)=\frac{1}{\varepsilon k}\Theta''_{f1}(Y)+\omega_f\,, \tag{44}$$

and the fluid phase energy equation in the porous region becomes

$$\frac{U_p}{\overline{U}}(1+\gamma+\omega_f+S\omega_s)=\frac{1}{k}\Theta''_{f2}(Y)+Bi\left(\Theta_s(Y)-\Theta_{f2}(Y)\right)+\omega_f. \tag{45}$$

Further, the solid phase energy equation in the porous insert is written as

$$0=\Theta''_s(Y)-Bi(\Theta_s(Y)-\Theta_{f2}(Y))+\omega_s. \tag{46}$$

The corresponding energy boundary conditions are

$$\Theta'_{f1}(1)=\varepsilon k, \tag{47a}$$

$$\Theta_{f1}(S)=\Theta_{f2}(S), \tag{47b}$$

$$\Theta'_{f2}(0)=\Theta'_s(0)=0, \tag{47c}$$

$$\Theta'_{f2}(s)=k\gamma, \tag{47d}$$

$$\Theta'_s(s)=\gamma, \tag{47e}$$

$$\Theta''_s(s)+Bi\,\Theta_{f2}(s)+\omega_s=0, \tag{47f}$$

$$\Theta_s(s)=0. \tag{47g}$$

By taking the second derivative of Eqs. (45) and (46) with respect to *Y*, the following expressions are obtained

$$\Theta''''_{f2}(Y)-Bi(1+k)\Theta''_{f2}(Y)=\frac{k}{\overline{U}}(1+\gamma+\omega_f+S\omega_s)(-BiU_p(Y)+U''_p(Y)+Bi\cdot k\cdot(\omega_f+\omega_s), \tag{48}$$

$$\Theta''_s(Y)-Bi(1+k)\Theta''_s(Y)=-\frac{Bi.k}{\overline{U}}(1+\gamma+\omega_f+S\omega_s)U_p(Y)+Bi\cdot k\cdot(\omega_f+\omega_s). \tag{49}$$

The second and third derivatives of Θ_s and Θ_{f2} at Y=0 are evaluated through the application of Eq. (47). This results in

$$\Theta'''_{f2}(0)=k\frac{U'_p(0)}{\overline{U}}=0, \tag{50a}$$

$$\Theta''_s(0)=0. \tag{50b}$$

Eventually, solving the ordinary differential Eq. (44) yields the following analytical relations for the temperature distribution of the flow in the open region

$$\Theta_{f1}(Y)\big|_{\text{ModelB}}=\frac{\varepsilon k}{\overline{U}}(1+\gamma+\omega_f+S\omega_s)(-\frac{1}{24}Y^4+A\frac{Y^3}{6}+B\frac{Y^2}{2})-\varepsilon\cdot k\cdot\omega_f\cdot\frac{Y^2}{2}+O_1Y+O_2, \tag{51a}$$

$$O_1 = \varepsilon \cdot k - \frac{\varepsilon k}{\overline{\overline{U}}}(1+\gamma+\omega_f+S\omega_s)(-\frac{1}{6}+\frac{A}{2}+B)+k\cdot\varepsilon\cdot\omega_f, \tag{51b}$$

$$O_2 = \Theta_{f2}(s) - \frac{\varepsilon k}{\overline{\overline{U}}}(1+\gamma+\omega_f+S\omega_s)(-\frac{1}{24}S^4+A\frac{S^3}{6}+B\frac{S^2}{2}) - O_1 S, \tag{51c}$$

in which *A* and *B* are respectively given by Eqs. (24) and (25). Solving Eqs. (48) and (49) and applying the boundary conditions (47) and (50) reveals the temperature distributions in the porous region. These are given by the following expressions

$$\Theta_{f2}(Y)\Big|_{\text{ModelB}} = \frac{\phi 1}{\Gamma^2}\cosh(\Gamma Y) + \left[-\frac{Bi\cdot k\cdot(\omega_f+\omega_s)}{\Gamma^2}+\frac{\frac{k}{\overline{\overline{U}}}(1+\gamma+\omega_f+S\omega_s)Bi\,Da}{\Gamma^2}\right]\frac{Y^2}{2} - \frac{\frac{k}{\overline{\overline{U}}}(1+\gamma+\omega_f+S\omega_s)C(Z^2-Bi)}{Z^2(Z^2-\Gamma^2)}\cosh(ZY)+\phi 3, \tag{52}$$

$$\Theta_s(Y)\Big|_{\text{ModelB}} = \frac{\phi 2}{\Gamma^2}\left[\cosh(\Gamma Y)-\cosh(\Gamma S)\right] + \frac{Bi\frac{k}{\overline{\overline{U}}}Da(1+\gamma+\omega_f+S\omega_s)-Bi\cdot k\cdot(\omega_f+\omega_s)}{\Gamma^2}\left[\frac{Y^2}{2}-\frac{S^2}{2}\right] - \frac{Bi\,C\frac{k}{\overline{\overline{U}}}(1+\gamma+\omega_f+S\omega_s)}{Z^2(Z^2-\Gamma^2)}\left[\cosh(ZY)-\cosh(ZS)\right], \tag{53}$$

where

$$\phi 1 = \frac{\Gamma}{\sinh(\Gamma S)}\left[k\gamma - \frac{Bi\cdot Da\frac{k}{\overline{\overline{U}}}(1+\gamma+\omega_f+S\omega_s)}{\Gamma^2}S+\frac{k(\omega_f+\omega_s)Bi}{\Gamma^2}S - \frac{\frac{k}{\overline{\overline{U}}}\cdot(1+\gamma+\omega_f+S\omega_s)\cdot C(Z^2-Bi)}{Z(Z^2-\Gamma^2)}\sinh(ZS)\right], \tag{54a}$$

$$\phi 2 = \frac{\Gamma}{\sinh(\Gamma S)}\left[\gamma - \frac{BiDa\frac{k}{\overline{\overline{U}}}\cdot(1+\gamma+\omega_f+S\omega_s)}{\Gamma^2}S+\frac{Bi\cdot k\cdot(\omega_f+\omega_s)}{\Gamma^2}S + \frac{Bi\frac{k}{\overline{\overline{U}}}\cdot(1+\gamma+\omega_f+S\omega_s)C}{Z(Z^2-\Gamma^2)}\sinh(ZS)\right], \tag{54b}$$

$$\phi 3 = \cosh(\Gamma S)\left[-\frac{\phi 1}{\Gamma^2} - \frac{\phi 2}{Bi}\right] + \frac{BiDa\frac{k}{\overline{\overline{U}}}\cdot(1+\gamma+\omega_f+S\omega_s)}{\Gamma^2}\left(-\frac{1}{Bi} - \frac{S^2}{2}\right) + \frac{k\cdot Bi(\omega_f+\omega_s)}{\Gamma^2}\left(\frac{1}{Bi} + \frac{S^2}{2}\right) + \frac{\frac{k}{\overline{\overline{U}}}\cdot(1+\gamma+\omega_f+S\omega_s)BiC}{Z^2(Z^2-\Gamma^2)}\cosh(ZS) - \frac{\omega_s}{Bi}, \tag{54c}$$

$$\Gamma = \sqrt{Bi\,(1+k)}. \tag{54d}$$

and *A*, *B* and *C* are provided by Eqs. (24), (25) and (27).

2.4.3 LTE solution

Adding Eqs. (34) and (35) results in

$$\frac{1}{k}\Theta_{f2}''(Y) + \Theta_s''(Y) + \omega_f + \omega_s = \frac{u_p}{\overline{U}}\left(1 + \omega_f + S\omega_s\right). \tag{55}$$

Under the local thermal equilibrium condition $\Theta_f = \Theta_s = \theta$. Hence, the one-equation model can be expressed as:

$$\left(\frac{1}{k} + 1\right)\Theta'' = \frac{u_p}{\overline{U}}\left(1 + \omega_f + S\omega_s\right) - (\omega_f + \omega_s), \tag{56}$$

subjected to the following boundary condition

$$\frac{\partial\Theta}{\partial Y}(y = 0) = 0, \qquad \Theta(Y = S) = \Theta_{f1}(S). \tag{57}$$

Integrating Eq. (56) and implementing boundary conditions (57), result in the following LTE temperature distribution,

$$\Theta(Y) = \frac{k}{1+k}\left\{\frac{1}{\overline{U}}\left[\frac{C}{Z^2}(\cosh(ZY) - \cosh(Z)) + \frac{1}{2}Da.(Y^2 - S^2)\right]\left(1 + \omega_f + S\omega_s\right) - \frac{1}{2}\left(\omega_f + \omega_s\right)(Y^2 - S^2)\right\}. \tag{58}$$

2.6 Validation

It can be readily demonstrated that by setting $\omega_f = \omega_s = 0$ in Eqs. (3) to (54) they reduce to the corresponding equations derived previously for non-heat-generating systems [37,38]. Hence, in this limit the developed solutions reduce to those of forced convection in a partially filled channel, derived previously by Karimi et al. [38] and other authors [36,37]. Further, for non-zero internal heat generations, Appendix A shows that the temperature fields in Eqs. (42), (43), (52), (53) and (58) can be systematically reduced to those reported by Yang and Vafai [24] for a fully filled channel with a Darcian flow. The analytical solution of Yang and Vafai [24] effectively assumes extremely small Darcy number, and hence

is less complicated than the derived temperature fields in section 2. It is demonstrated in Appendix A that in the case of very low permeability and a fully-filled channel, the temperature fields derived in section 2.4 become identical to those in Ref. [24]. It is interesting to note that in the solution of Yang and Vafai the energy source term of the fluid phase has no influence upon the non-dimensional temperature fields. This is clearly not the case in the present problem. By considering a partially filled channel and the Darcy-Brinkman model in the current study, energy source terms in both solid and fluid phases remain influential. Appendix A, further shows that LTE solutions of section 2.4.3 can be converted to their low permeability and full porous equivalent, derived by Yang and Vafai [24].

3. Results and discussion

Table 1: Internal heat sources of the investigated cases

	Case1	Case 2	Case 3	Case 4
ω_f	0	10	10	-10
ω_s	10	0	-10	10

Four different cases of internal heat generation and consumption are considered (see Table 1). In keeping with the literature [24], the non-dimensional energy source terms are of order 10. In case 1, heat generation is limited to the solid matrix. Obvious practical examples of this case can be found in electronic cooling and nuclear technology. In case 2, heat is generated only in the fluid phase. This is representative of a broad range of problems, in which the fluid phase features an exothermic chemical reaction. Cases 3 and 4 correspond to the situations in which, heat is generated in one phase while it is consumed in the other phase at the same intensity. Heat consumption could be due to endothermic chemical reactions occurring in either the solid or fluid phase. These cases can be readily extended to other combinations of the energy source terms in the fluid and solid phases. This extension is, to some extent, done in section 3.4. Here, the main rationale behind the selection of cases 1-4 lies in isolating the source term for one phase cases (1 and 2) and equating the exothermic and endothermic intensities in the two phase cases (3 and 4). The discussions in this section are focused on the behaviour of the temperature fields and the validity of local thermal equilibrium as a simplifying assumption. Furthermore, special attention is paid to the interface of the porous insert by examining the possibility of temperature gradient bifurcation. In all results presented in this section the porosity of the investigated porous medium is set to 0.5. Thus, throughout this section the volumes of the solid and fluid phase in the porous region are equal.

3.1 Heat flux distribution

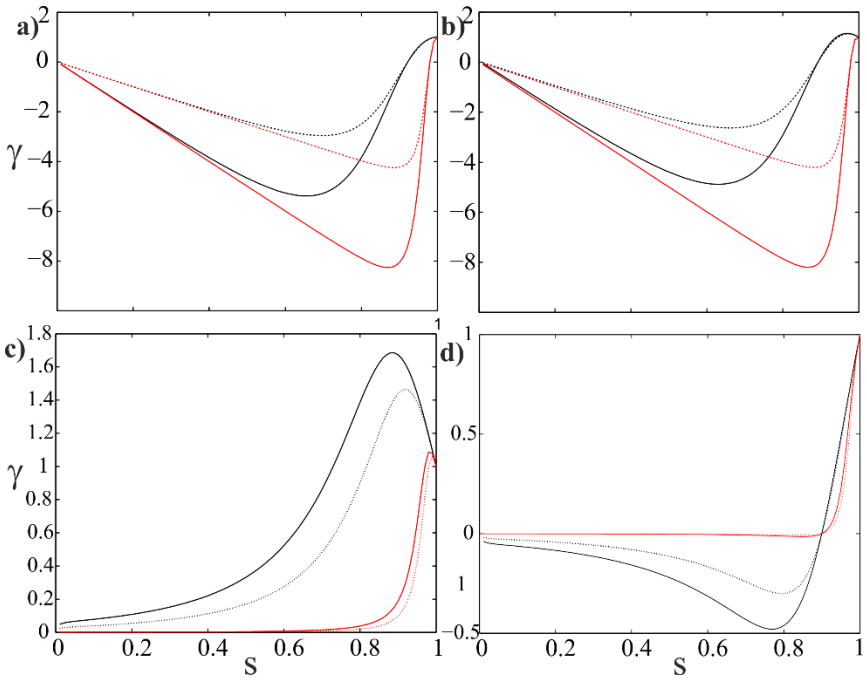

Fig 2. Heat flux distributions at varying porous insert thickness, red line: Da=10^{-5}, black line: Da=10^{-3}, solid line: model A, dotted line: model B, a) case1: $\omega_f = 0,\ \omega_s = 10$, b) case2: $\omega_f = 10, \omega_s = 0$, c) case3: $\omega_f = 10, \omega_s = -10$, d) case4: $\omega_f = -10, \omega_s = 10$.

Figures 2a-d show variations in the ratio of the wall heat flux to that of the interface (γ in Eqs. 30 and 32) against the thickness of the porous insert and for a wide range of Darcy number values. This figure shows that at low values of porous thickness, and regardless of the internal heat sources, the heat flux ratio for each interface model becomes less dependent upon Darcy number and interface model. This is in keeping with the previous results for non-heat-generating systems [38]. However, compared to those cases, the heat flux ratios in Fig. 2 show noticeably more complex behaviours. In this figure, the heat flux ratios reach local maxima/minima at certain values of the porous insert. The precise values of the thickness, at which the heat flux ratios reach their extremum, are heavily dependent upon the Darcy number and generally decreases as the Darcy number increases. It is also observed that model A always predicts a smaller extremum thickness. Furthermore, as expected, in all investigated cases predictions using both models converge at high values of the thickness and become equal to that of the channel wall.

Interestingly, exothermicity and endothermicity in solid and fluid phases can cause negative values of the heat flux ratio (see Figs. 2a,b and d). This means that while heat is added to the channel wall, the

interface of the porous insert loses heat. Such behaviour seems to be exclusive to the systems with internal heat sources and has not been previously reported. Further, Figs. 2a and b indicate that internal heat generations in either of solid or fluid phase have similar effects upon the heat flux ratio. However, different combinations of heat generation and consumption in solid and fluid phases, as shown in Figs 2c and d, can significantly modify the heat flux ratio. Importantly, the sign of heat flux ratio can vary as heat is generated and consumed in the fluid or solid phases. These figures reflect the complexities of cases 3 and 4. Although solid and fluid phases have equal volumes and opposite energy sources, the heat flux distributions in cases 3 and 4 are clearly different. This is due to the effect of energy released/consumed in the open region which affects the delivery of heat flux to the interface.

3.2 Temperature distributions under models A and B, and local thermal equilibrium

Figures 3 to 6 show the temperatures of fluid and solid phases, in the porous region with varying values of conductivity ratio and Biot number. These are predicted under the two interface models and for the four cases listed in Table 1. Further, these figures include the LTE temperature field (Eq. 58) and the fluid temperature in the open region. The non-dimensional value of the porous thickness in Figs. 3 to 6 is 0.7.

Figure 3 corresponds to case 1 in Table 1, in which heat is only generated within the solid phase. This figure shows that, under model A, the fluid and solid temperatures remain relatively close to each other. This remains true for all combinations of Biot and conductivity ratio (solid black line and dotted line). Model B, however, predicts a significant temperature difference between the solid and fluid phases for low values of Biot number (dotted-dashed line and dashed line in Figs. 3a and 3c). As the numerical value of Biot number increases in Figs. 3b and 3d this behaviour changes, and the fluid and solid temperatures, under model B (dotted-dashed line and dashed line), approach each other. This is to be expected, as higher value of Biot number implies stronger internal heat exchange between the fluid and solid phases. Hence, the temperature difference between the two phases declines. In general, the observed trend in the temperature distributions in Fig. 3 is consistent with the corresponding non-heat-generating case [37]. Figure 3, further, shows the influence of Biot number upon the temperatures of fluid in the open region. At low Biot numbers, there are substantial differences between the temperature of the open fluid (blue solid and dotted-dash lines), and subsequently the wall temperatures, under models A and B. The extent of these differences substantially declines as Biot number increases in Figs. 3b and 3d.

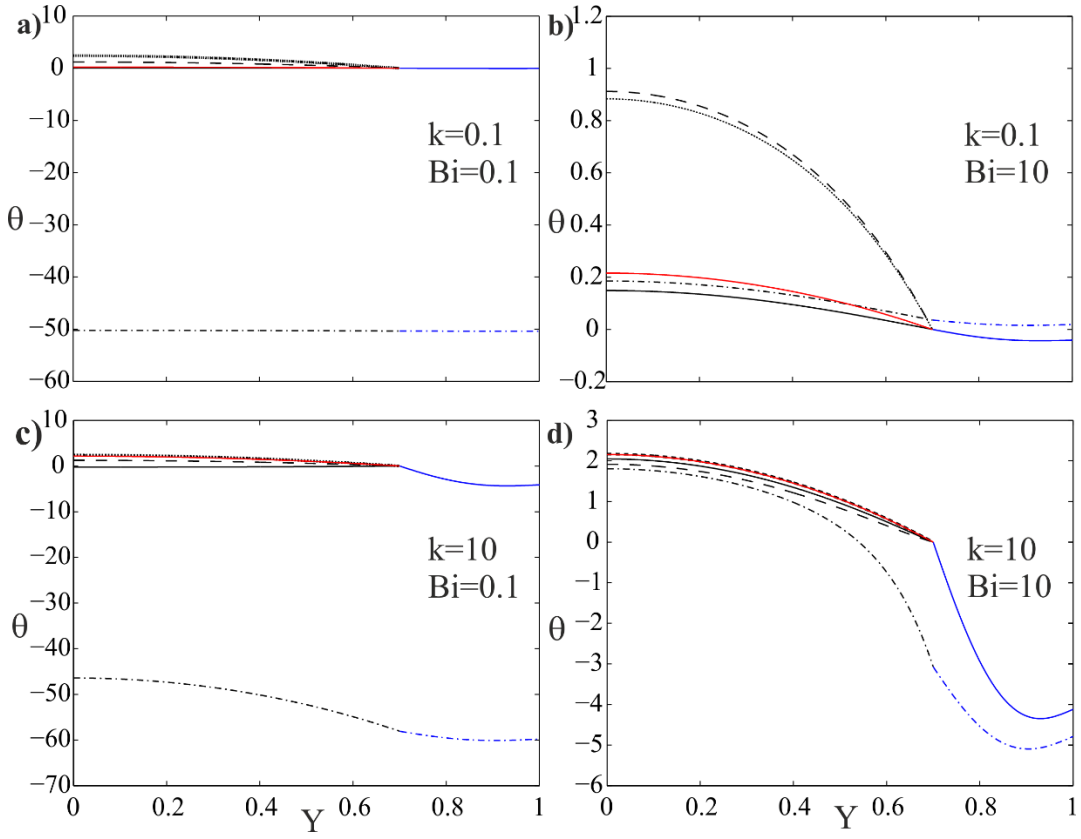

Fig. 3. Non-dimensional temperature profiles at S=0.7 and Da=10^{-3}, case1: $\omega_f = 0, \omega_s = 10$, red line: LTE, solid black line: $\Theta_{f2}\big|_{\text{ModelA}}$, dotted line: $\Theta_s\big|_{\text{ModelA}}$, dotted-dash line: $\Theta_{f2}\big|_{\text{ModelB}}$, dashed line: $\Theta_s\big|_{\text{ModelB}}$, blue solid line: open fluid temperature under model A, blue dotted-dash line: open fluid temperature under model B.

Figure 4 shows the case with heat generation within the fluid phase only (case 2 of Table 1). It is clear that this figure features a few distinctions and similarities with respect to case 1 (shown in Fig.3). In the limiting case of low Biot number, it is noted that in contrast to Fig. 3a and 3c, the values of temperature in Figs 4a and c are all positive. Similar to case 1, however, Fig. 4a shows small temperature difference between the solid and fluid phases under model A, and a large disparity between these two under model B. Nonetheless, as the value of the conductivity ratio increases (Fig 4c), regardless of the interface model, the temperature difference between the fluid and solid phases becomes significant. This is such that in Fig. 4c there is always a significant difference between the LTE and LTNE predictions of the fluid temperature. Once again, at higher values of Biot number (Figs 4b and d) all fluid and solid phase temperature predictions approach each other. This trend appears to be slightly weaker than that observed

in case 1 (Figs. 3b and d). As a result, local thermal equilibrium seems to be only a crude approximation in this high Biot number limit. Similar to that observed in Fig. 3, at low Biot number the open fluid temperature shows a high sensitivity to the interface model. However, the open fluid temperatures under models A and B approach each other in the limit of high Biot number. Consequently, in Fig. 4d models A and B predict similar wall temperatures at Y=1.

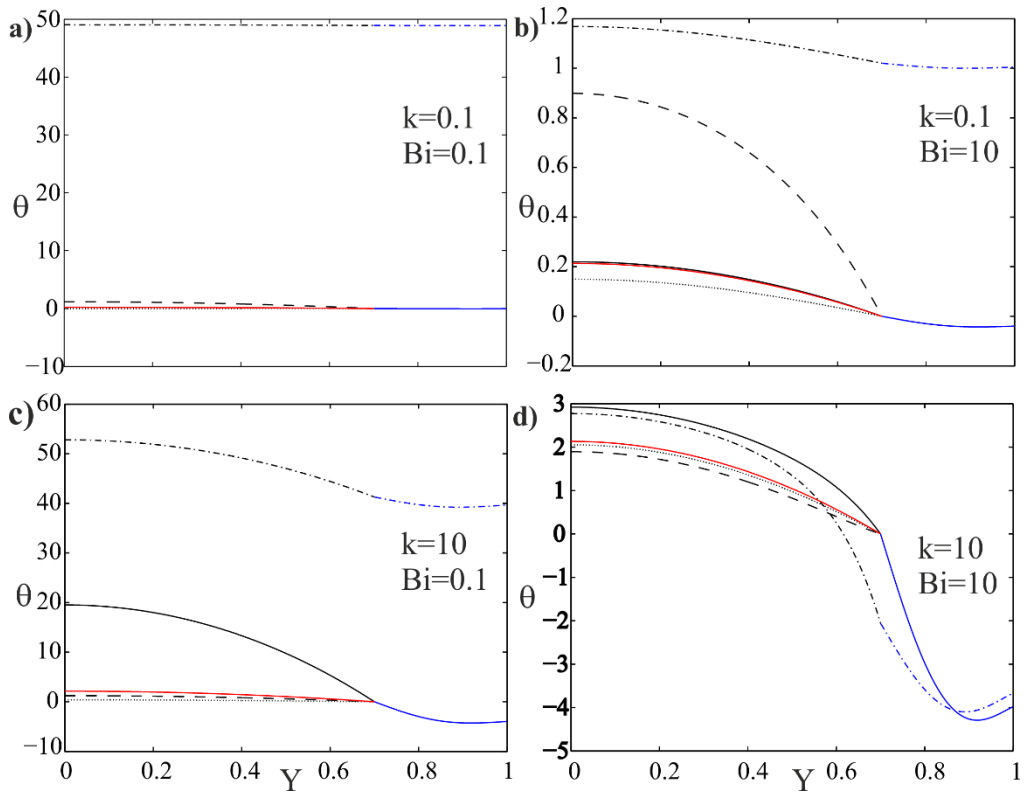

Fig. 4. Non-dimensional temperature profiles at S=0.7 and Da=10^{-3} , case2: $\omega_f = 10, \omega_s = 0$, red line: LTE, solid black line: $\Theta_{f2}\big|_{\text{ModelA}}$, dotted line: $\Theta_s\big|_{\text{ModelA}}$, dotted-dash line: $\Theta_{f2}\big|_{\text{ModelB}}$, dashed line: $\Theta_s\big|_{\text{ModelB}}$, blue solid line: open fluid temperature under model A, blue dotted-dash line: open fluid temperature under model B.

Figures 5 and 6 correspond to cases 3 and 4 in Table 1. In these cases, thermal energy is produced in one phase while it is consumed in another phase with the same intensity. It should be noted that in the present cases the volumes of the fluid and solid phases are the same (ε=0.5). Hence, the generated and consumed thermal energies within the porous region cancel each other. It is clear that in Figs. 5 and 6 the LTE prediction of temperature remains close to zero. This indicates that under the local thermal equilibrium assumption the porous region remains essentially isothermal and there is little temperature gradient within

the region. This is in clear contrast to the LTE predictions in the previous cases (see Figs.3d and 4d), in which spatial variation of LTE temperature is conspicuous. Another distinctive feature in Figs. 5 and 6 is the constancy of the solid and fluid phase temperature in the porous medium under model B. This is different to that observed in Figs. 3 and 4. Further, it appears that the temperature fields in Figs. 5 and 6 are almost mirror reflection of each other. It is shown in the following section that as the thickness of the porous insert varies, this symmetry breaks down. It is, further, clear from Figs. 5 and 6 that for low Biot number and conductivity ratio (Figs. 5a and 6a) the outcomes of model A are reasonably close to LTE predictions. Model B, however, predicts substantially different temperatures for the solid and fluid phases. This trend is similar to that observed in cases 1 and 2 (see Figs. 3a and 4a) and also the non-heat-generating case [37]. Increasing the conductivity ratio and keeping Biot number constant in Figs. 5c and 6c appear to have no visible influence upon the predictions of model B. Nonetheless, model A predicts that the fluid temperature in the core of the porous region is now considerably different to that of the solid phase. This difference diminishes towards the surface of the porous insert and, as required by model A, the fluid and solid phase temperatures become identical on the interface. Increasing the Biot number in Figs. 5b and d and, Figs. 6b and d causes a significant reduction in the temperature differences under both interface models. By increasing the Biot number, the convective heat transfer coefficient between the fluid and solid matrix increases. Hence, the temperature difference between the two phases diminishes.

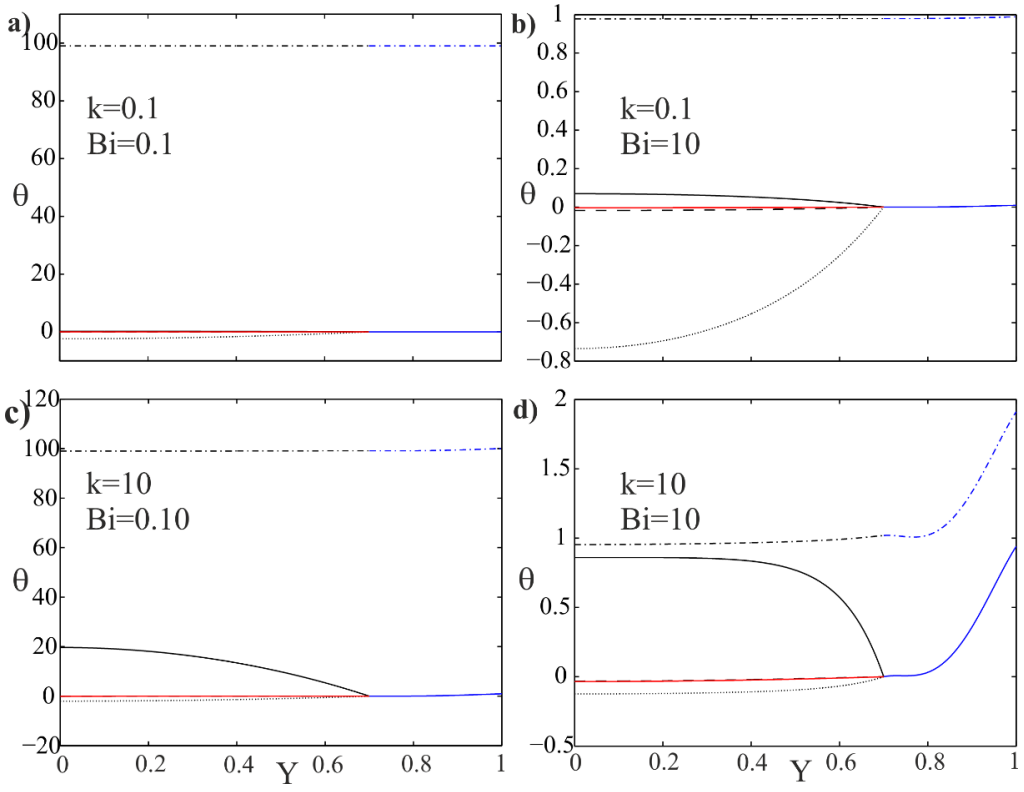

Fig. 5. Non-dimensional temperature profiles at S=0.7 and Da=10^{-3}, case3: $\omega_f = 10, \omega_s = -10,$ red line: LTE, solid black line: $\Theta_{f2}\big|_{\text{ModelA}}$, dotted line: $\Theta_s\big|_{\text{ModelA}}$, dotted-dash line: $\Theta_{f2}\big|_{\text{ModelB}}$, dashed line: $\Theta_s\big|_{\text{ModelB}}$, blue solid line: open fluid temperature under model A, blue dotted-dash line: open fluid temperature under model B.

Overall, Figs. 3 to 6 show that the existence of exothermicity or endothermicity in the porous region can significantly modify the temperature fields. Comparing with the non-heat-generating case, the validity of LTE becomes highly questionable. Even at the high Biot number limit where the temperature differences between the two phases are relatively small, they are still considerably larger than their corresponding values in non-heat-generating cases. It follows that for the system under investigation, LTE is only a crude approximation, which can be used when there exist a strong heat exchange between the two phases. Previous studies [37] have shown that by decreasing the Darcy number, and therefore the permeability, LTE condition is approached. This is, primarily, due to the reduced filtration velocity and therefore increased fluid residence time in the porous region, which enhances the internal heat exchange process. Although not shown, the same qualitative trend was observed here as Darcy number was reduced to Da=10^{-4}. Importantly, reducing Darcy number did not change the qualitative shape of the temperature distribution in Figs. 3-6. Yet, the temperature differences were still considerably larger than that in the corresponding non-heat-generating case.

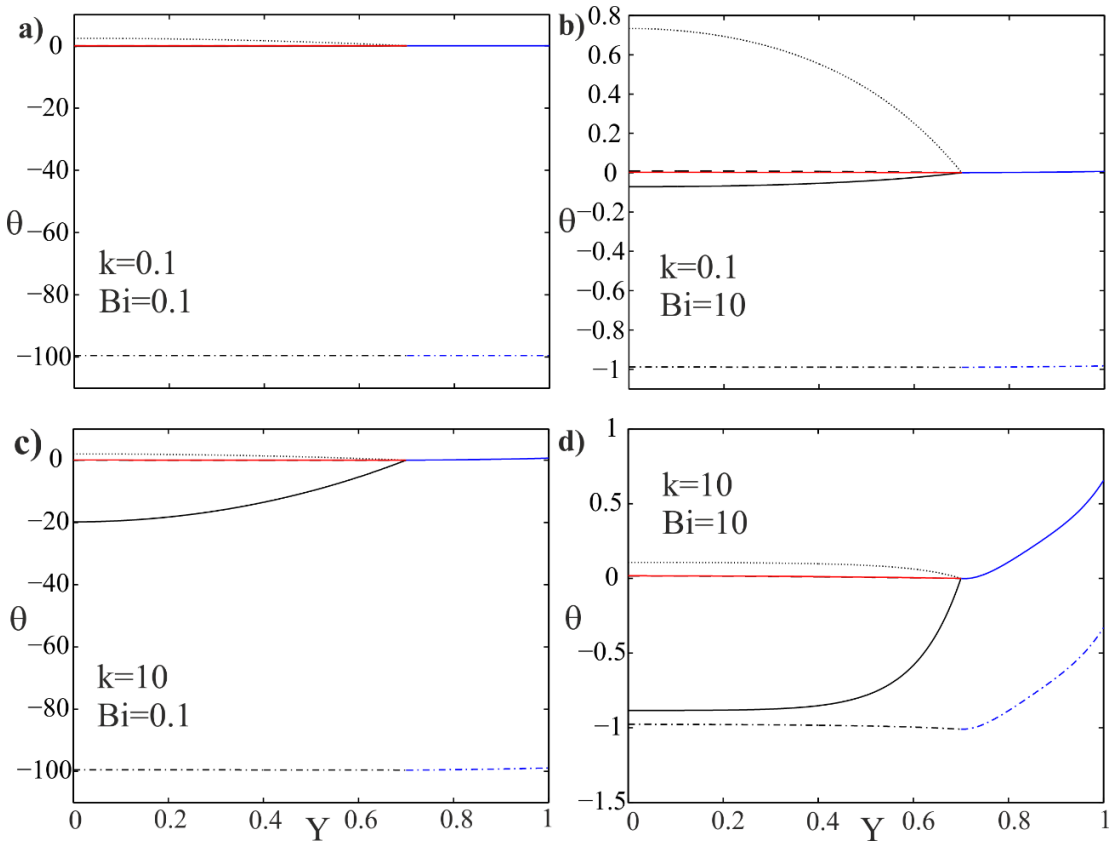

Fig. 6. Non-dimensional temperature profiles at S=0.7 and Da=10^{-3}, case4: $\omega_f = -10, \omega_s = 10,$ red line: LTE, solid black line: $\Theta_{f2}\big|_{\text{ModelA}}$, dotted line: $\Theta_s\big|_{\text{ModelA}}$, dotted-dash line: $\Theta_{f2}\big|_{\text{ModelB}}$, dashed line: $\Theta_s\big|_{\text{ModelB}}$, blue solid line: open fluid temperature under model A, blue dotted-dash line: open fluid temperature under model B.

3.3 Maximum temperature difference between the solid and fluid phases

It is well documented that the maximum temperature difference between the fluid and solid phases in the porous insert depends upon a number of parameters [35,36]. These include Darcy number, thermal conductivity ratio, Biot number, thickness of the porous insert and, importantly, the porous-fluid interface model [35-37]. This section analyses the influence of exothermicity and endothermicity, in either of fluid or solid phase, upon the maximum temperature difference between the two phases.

Figure 7 shows the variation in the absolute value of the maximum temperature difference between the fluid and solid phases against all porous insert thicknesses for case 1. To generate this figure and Figs. 8-10 the maximum temperature difference between the two phases, within the porous region, was found at a

certain value of S. The process was then repeated for all values of S between 0 and 1. The predictions of both model A and B have been shown. Further, this figure includes the results for two different Darcy numbers, while different combinations of Biot number and conductivity ratio have also been considered. Figs. 7a indicates that at the limit of low Biot number and thermal conductivity ratio and under model A, the maximum temperature difference remains negligible up to S≈0.4. For greater thicknesses of the porous insert, there is a sizeable maximum temperature difference between the two phases, which appreciates as the non-dimensional porous thickness approaches one. This appears to be almost independent of the Darcy number. The same qualitative behaviour is observed at higher conductivity ratios (see Fig. 7c). However, increasing the conductivity ratio exacerbates model A temperature differences for thicker porous inserts. For low Bi and k, model B predicts a very large temperature difference for all values of the porous insert thickness (see Fig. 7a). As expected, increasing the value of

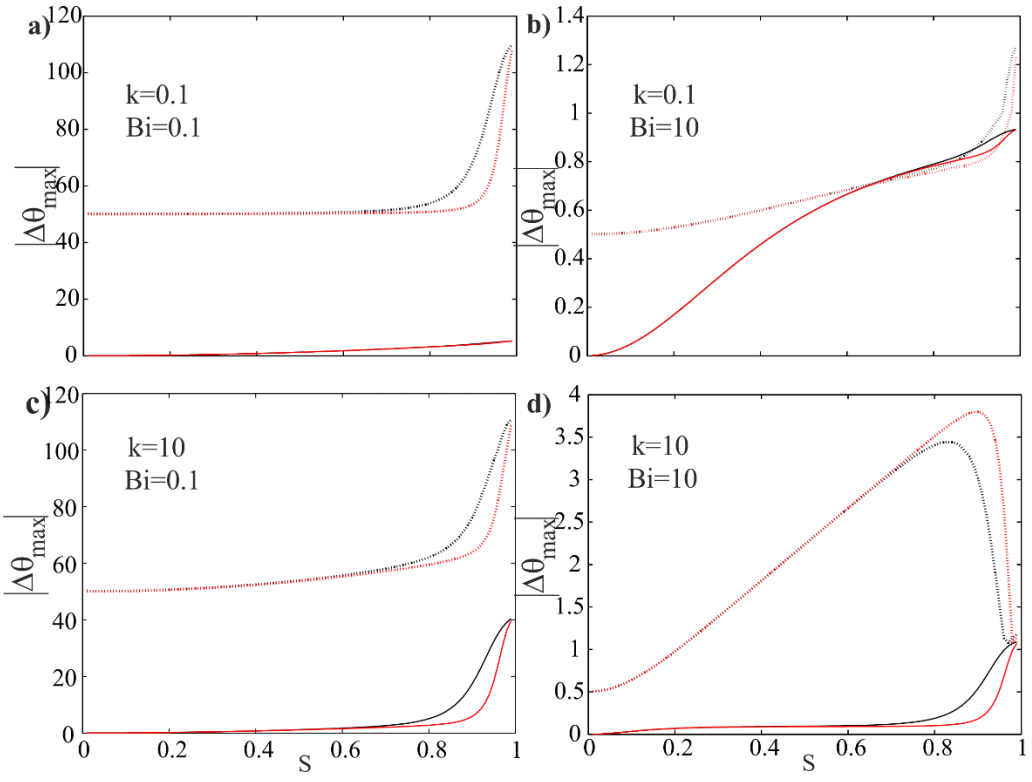

Fig. 7. Absolute value of the maximum temperature difference between the solid and fluid phases at varying thickness of the porous insert, case1: $\omega_f = 0, \omega_s = 10$, black lines: Da=$10^{-4}$, red lines: Da=$10^{-5}$, solid line: model A, dotted line: model B.

Biot number in Figs. 7b and 7d reduces the temperature differences predicted by models A and B. Similar, to that observed in Figs. 7a and c, regardless of the thickness of the porous insert, model B always predicts a finite temperature difference. However, under all values of Bi and k, model A gives negligible temperature difference for low values of the porous thickness. This temperature difference then becomes significant as the thickness of the porous insert increases. Figures 7a to d, further, show that generally the temperature difference between the two phases is smaller at lower Darcy number. An exception to this is model B prediction in Fig. 7d, in which low Darcy number prediction of the temperature difference exceeds that of the high Darcy number. Further, in this figure the temperature difference under model B goes through a sharp decrease at higher porous insert thicknesses.

As shown in Fig. 8, moving the exothermicity to the fluid phase (case 2 of Table 1) causes substantial changes in the behaviour of the maximum temperature difference. A distinctive feature of Figs. 8a-d is the prediction of a higher maximum temperature difference at lower Darcy number. The behaviour can be seen under both considered interface models and for all combinations of Biot number and conductivity ratio. This could be due to the fact that, in this case heat is generated in the fluid phase and therefore lower permeability and higher fluid residence time leaves an energy accumulative effect. Another clear feature in Figs 8a-d is the reduction of the maximum temperature difference at the values of S close to unity. It is observed that under both interface models the maximum temperature difference initially increases by the increase in the porous thickness. However, this trend is reversed at higher porous thickness and the maximum temperature differences sharply decrease and reach minima at values of S greater than 0.9. Further increase in the porous thickness increases the value of the maximum temperature difference. The reason for this complex behaviour is not immediately obvious and requires further investigations.

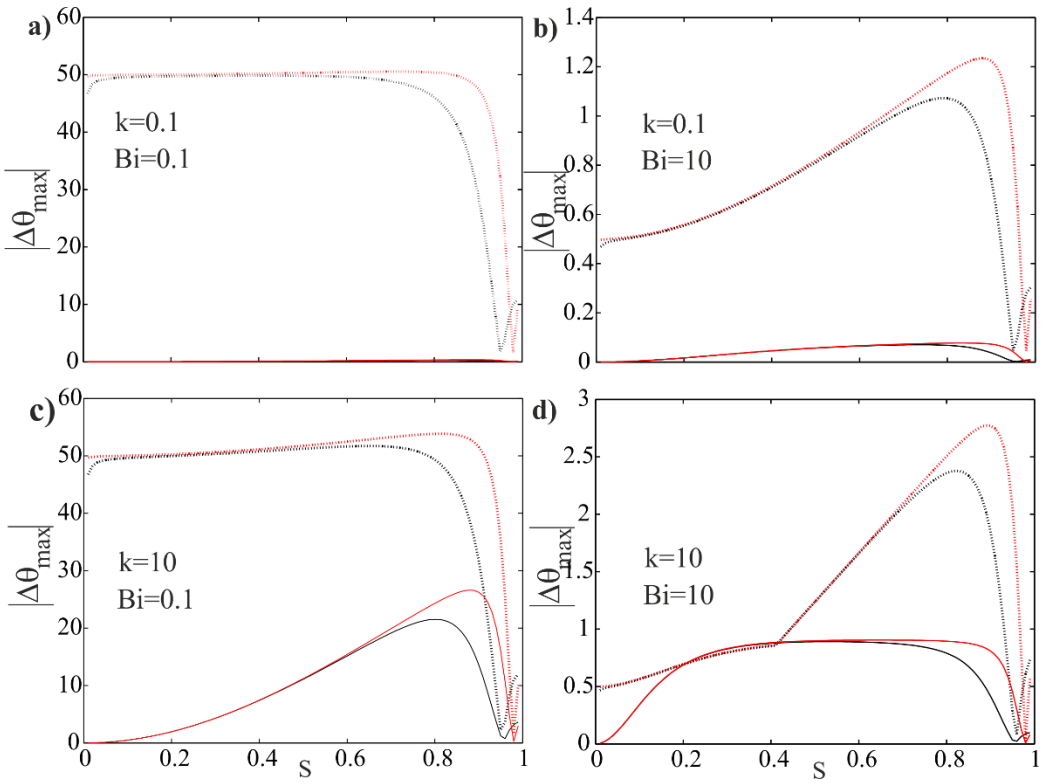

Fig. 8. Absolute value of the maximum temperature difference between the solid and fluid phases at varying thickness of the porous insert, case2: $\omega_f = 10, \omega_s = 0$, black lines: Da=$10^{-4}$, red lines: Da=$10^{-5}$, solid line: model A, dotted line: model B.

Combination of exothermicity and endothermicity, in cases 3 and 4 of Table 1, introduces new patterns in the graphs of maximum temperature difference. Figures 9 and 10 represent the maximum temperature difference between the two phases for cases 3 and 4. These figures show that the maximum temperature difference under model B remains, mostly, unchanged for almost all porous thicknesses and values of Biot number and conductivity ratio. Some increase and decrease of this value is observed at higher porous thickness. Yet, compared to Figs. 7 and 8 the, variations in the maximum temperature difference predicted by model B in Figs. 9 and 10 are much smaller. In keeping with the earlier findings of this article and those of others for non-heat-generating cases [38], the maximum temperature differences in Figs. 9 and 10 are higher at lower Biot numbers. At low values of Biot number and conductivity ratio, model A predicts small temperature differences for non-dimensional porous thickness less than 0.4. In this limit of Biot number and conductivity ratio the temperature difference calculated through model B is quite substantial. It is further noted that, in Figs. 9 and 10, the influence of Darcy number upon the maximum temperature difference is less pronounced compared to that in Figs. 7 and 8. This is particularly

the case in Fig. 10 in which there is nearly no difference between the maximum temperature differences predicted at different Darcy numbers. Further, at higher values of S the temperature difference in Figs. 9 and 10 are considerably different. For instance, a comparison between Figs. 9d and 10d reveals that for S>0.9 model B prediction of the temperature difference in case 3 is noticeably higher than that of case 4. Conversely, at this limit model A predicts a smaller temperature difference for case 3.

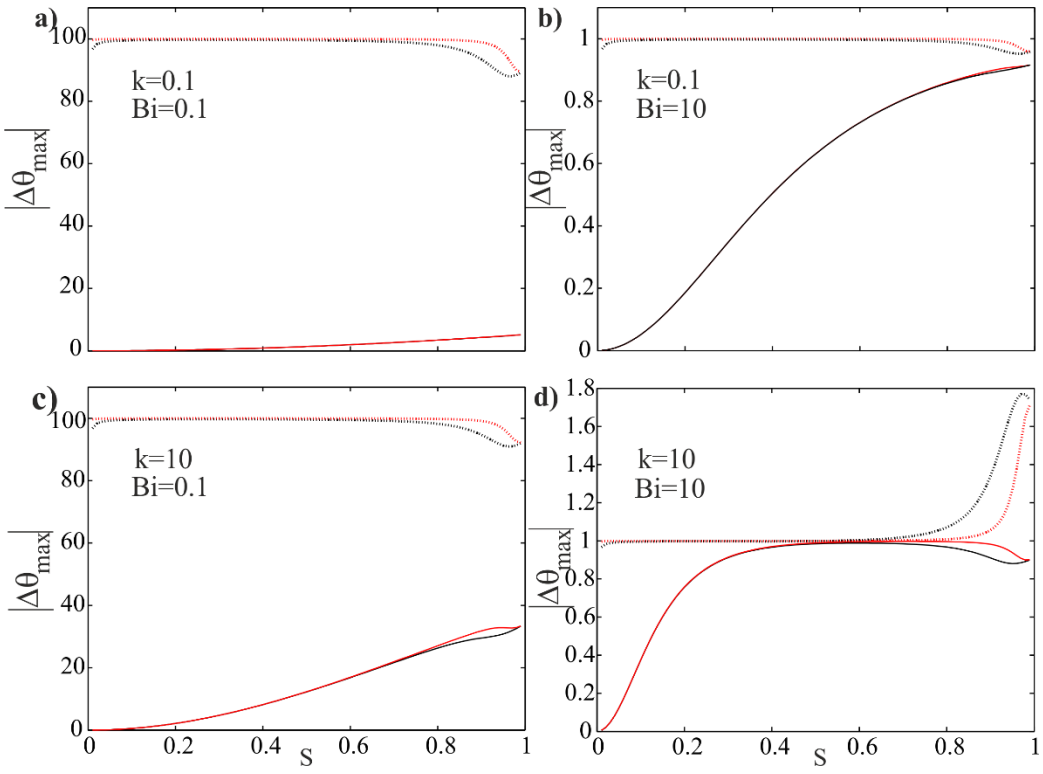

Fig. 9. Absolute value of the maximum temperature difference between the solid and fluid phases at varying thickness of the porous insert, case3: $\omega_f = 10, \omega_s = -10$, black lines: Da=$10^{-4}$, red lines: Da=$10^{-5}$, solid line: model A, dotted line: model B.

The presented analysis indicates that for almost all combinations of parameters, in all four considered cases, model B predicts greater values of temperature difference. The disparities between the predictions of model A and B in the limit of low Biot number is quite substantial. At high Biot numbers, however, there are regions of the porous insert thickness in which the predictions of the two models become similar. Further, as a general rule, for low values of the porous thickness the maximum temperature difference under model A is small. This is because by definition model A sets equal solid and fluid temperatures on the interface of the porous insert (see Eq. 12b). Hence, as the porous thickness

approaches zero the maximum temperature difference within the porous region becomes negligibly small. However, there is no such restriction in model B and therefore even at small porous insert thicknesses finite temperature differences can exist. It should be noted that as demonstrated previously [37], in the absence of the energy source terms the maximum temperature difference is only appreciable at higher value of the porous thickness. This remains the case for all combinations of the parameters and interface models for the case without internal energy sources [37]. Introduction of exothermicity and endothermicity, therefore, has a strong effect upon the temperature difference between the two phases. It follows that in the problems including internal energy generation, the application of local thermal equilibrium should be either avoided or practiced most carefully. Furthermore, the present findings clearly show the significance of the interface model upon the predicted temperature fields.

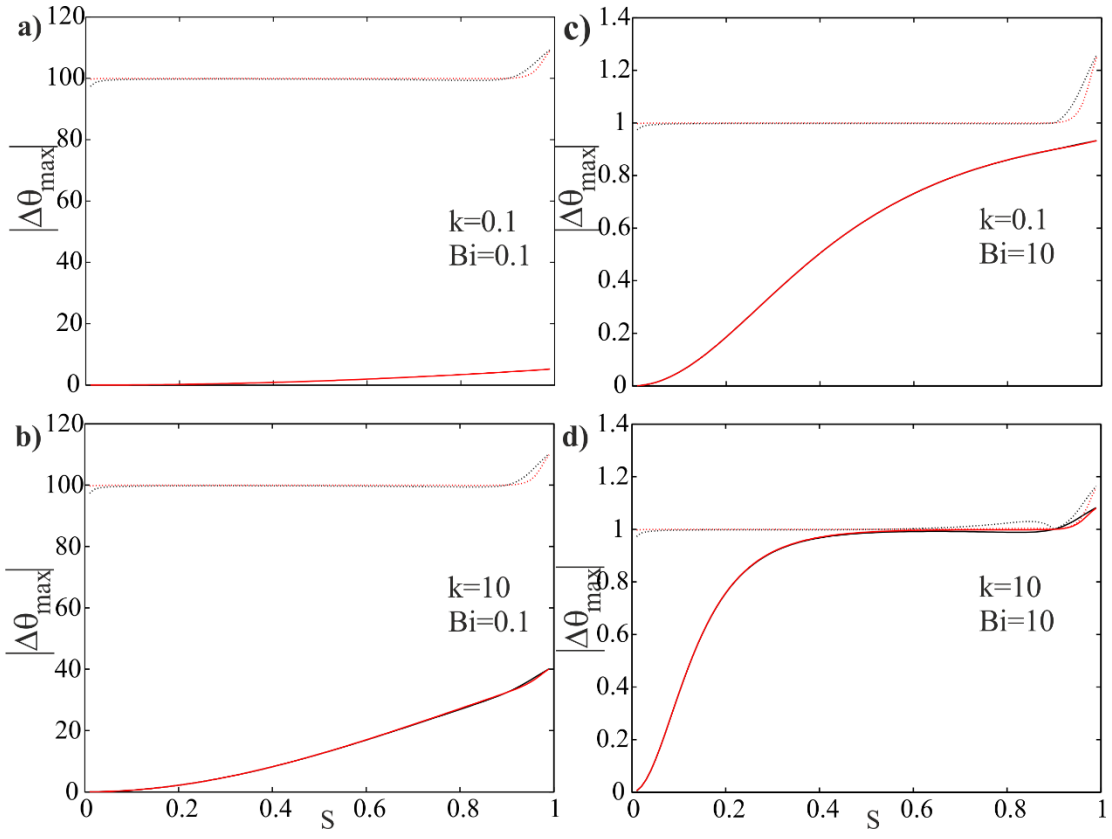

Fig. 10. Absolute value of the maximum temperature difference between the solid and fluid phases at varying thickness of the porous insert, case4: $\omega_f = -10, \omega_s = 10$, black lines: Da=$10^{-4}$, red lines: Da=$10^{-5}$, solid line: model A, dotted line: model B.

3.4. Temperature gradient bifurcation on the interface of the porous insert

The analyses, so far, presented in this article have been limited to the four cases detailed in Table 1. In practice, however, an infinite number of other combinations of ω_f and ω_s may occur. In addition to modifying the results of sections 3.1 to 3.3, variation of the energy source terms can introduce peculiarities in the thermal behaviour of the system. An example of these peculiar behaviours is given here through the study of the temperature gradient bifurcation on the porous-fluid interface. This effect includes a variation in the sign of the solid and fluid temperature gradients on the interface of the porous insert. Yang and Vafai [24] showed that bifurcation of the temperature gradient on the interface activates a new mechanism of internal heat exchange between the two phases. The temperature gradient bifurcation on the interface allows part of the heat to be conducted from the hotter phase into the interface and then from there to the colder phase [24]. Hence, the interface acts as an extra agent of heat exchange between the solid and fluid phase [24]. Examples of such situations can be seen in Figs. 5b, c and d in which the solid and fluid temperature gradients on the interface, are of different signs. Mathematically, the parameter Σ is defined as $\Sigma = \Theta'_{f2}(Y)\big|_{\text{Model A}} / \Theta'_{s}(Y)\big|_{\text{Model A}}$ (see Appendix B for the full analytical expressions). Thus, $\Sigma < 0$ indicates that the signs of fluid and solid temperature gradients on the interface are different and therefore the temperature gradient on the interface has bifurcated. Yang and Vafai [24] showed that this phenomenon can occur in internal heat generating porous media. It follows from the definition of the interface models (Eqs. 12 and 13) that temperature gradient bifurcation on the interface of the porous insert can only happen under model A. Application of model B automatically sets the signs of the temperature gradients the same and hence, removes the possibility of temperature gradient bifurcation.

Identification of the regions of the parametric space in which temperature gradient flux bifurcation occurs is of fundamental significance [24]. These regions can be identified through the use of the analytical solutions of the temperature fields developed in section 3 and Appendix B. Figure 11 shows an example of such identification process. Each image in this figure corresponds to a pair of non-dimensional internal energy generation/consumption. For a given Darcy number, porous thickness and internal energy generations, the sign of Σ can be evaluated over a wide range of Biot number and conductivity ratio. Some specific combinations of ω_f and ω_s feature heat bifurcation over a part of the Bi-k plane.

Figure 11 clearly shows that the occurrence of temperature gradient bifurcation is heavily dependent upon the energy source terms. This is such that a small variation in the strength of these terms can significantly affect the parametric region over which this bifurcation occurs. For instance, a slight intensification of the exothermicity from Fig.11a to Fig. 11b highly widens the region of temperature gradient bifurcation. In

another example, increasing the intensity of exothermicity in the solid phase from Fig. 11c to Fig. 11f extends the bifurcation to almost the entire surface of the Bi-k plane. However, signifying the fluid phase exothermicity between Fig.11d and Fig. 11e has a relatively small effect upon the regions of temperature gradient bifurcation. This sensitivity of heat bifurcation upon the internal heat generations indicates the importance of the close evaluation of this effect at any given set of parameters. The analytical expressions presented in Appendix B can greatly facilitate such evaluation.

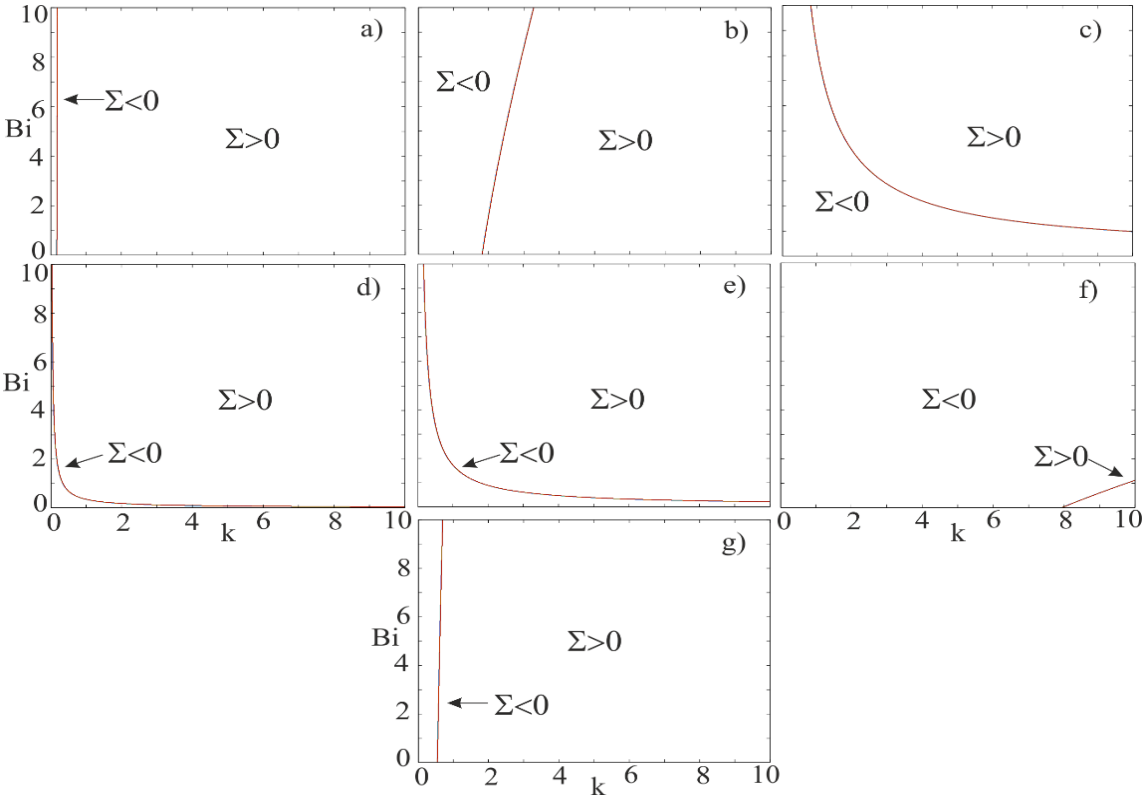

Fig. 11. Bifurcation of heat on the interface of the porous insert for varying combinations of solid and fluid internal heat generation, Da=10^{-4}, S= 0.7, model A. a) $\omega_f = 0$ & $\omega_s = -10$, b) $\omega_f = 2$ & $\omega_s = -10$, c) $\omega_f = -10$& $\omega_s = 2$, d) $\omega_f = 200$ & $\omega_s = -10$, e) $\omega_f = 20$ & $\omega_s = -10$, f) $\omega_f = -10$ & $\omega_s = 20$, g) $\omega_f = -10$ & $\omega_s = 200$.

4. Conclusions

Analytical solutions were developed for the solid and fluid temperature fields in a channel with a partial fill of porous material under constant wall heat-flux and fully-developed conditions. The flow was assumed to be laminar and compressible. The fluid and solid phases in this system were also allowed to display internal energy generation or consumption. A two-equation model of energy transport,

representative of the local thermal non-equilibrium (LTNE) assumption, along with the Darcy-Brinkman model of momentum transfer were used to formulate the problem. The thermal boundary condition on the porous-fluid interface was described using two existing interface models (models A and B). Further analytical results were developed by assuming local thermal equilibrium (LTE) and solving the "one-equation" energy transport model. The developed solutions were shown to be asymptotically equivalent to the existing derivations of the temperature fields for a fully filled channel with low permeability. It was demonstrated that both fluid and solid thermal sources are of significance in determining the thermal behaviour of the system under investigation. This was different to that reported earlier [24] for a fully filled channel with a Darcian flow in which only heat source in the solid phase affects the dimensionless temperatures. The LTE and LTNE predictions of the temperature fields were compared with each other over a wide range of pertinent parameters. These included Darcy and Biot numbers, conductivity ratio, porous insert thickness, internal energy sources and interface models. It was shown that, in general, at low Biot numbers and regardless of the energy sources, the difference between the LTE and LTNE predictions was quite significant. This difference diminished at higher Biot numbers. It was observed that variations in Darcy number in those cases incorporating internal energy sources could either increase or decrease the temperature difference between the two phases. Further, the analyses presented in this article showed that in heat generating systems model B generally predicted a greater temperature difference between the two phases. In these systems LTE could be an acceptable approximation only for small thicknesses of the porous insert and high Biot numbers. Temperature gradient bifurcation on the surface of the porous insert was further studied as a phenomenon occurring in systems with internal heat generation. It was shown that variations in the energy sources in either solid and/or fluid phase could significantly affect the occurrence of this phenomenon.

Appendix A. Asymptotic behaviour of the analytical solution in the limit of fully-filled duct ($S = 1$) and plug flow ($Da \to 0$)

This appendix shows that the analytical expressions derived in section 2.4 for the solid and fluid temperature fields can be rigorously reduced to those reported earlier by Yang and Vafai [24]. In the followings, the asymptotic behaviour of the derived temperature fields in the limits of extremely small permeability and fully filled channel is analysed. These are the conditions under which Yang and Vafai [24] derived their results.

The porous insert is, first, expanded to occupy the whole duct volume (S = 1) while Darcy number approaches zero. Substituting S =1 into Eq. (24) and (25) leads to

$$A = 1 - Da \times Z \times \tanh(Z), \tag{A1a}$$

$$B = -1/2 + Da \times Z \times \tanh(Z), \tag{A1b}$$

and hence, constant C in Eq. 27 becomes

$$C = -\frac{Da}{\cosh(Z)}. \tag{A1c}$$

Therefore, the velocity in the porous medium given by Eq. 26 takes the form of

$$U_p = Da\left[1 - \frac{\cosh(ZY)}{\cosh(Z)}\right]. \tag{A1d}$$

Substitution of C and S = 1 into Eq. (28) gives the average velocity as

$$\bar{U} = Da\left[1 - \frac{\tanh(Z)}{Z}\right]. \tag{A1e}$$

For very small Darcy number the value of $Z = 1/\sqrt{Da}$ is very large, Γ^2 and Bi are negligible compared to Z. Further, for large Z, $\frac{\cosh(ZY)}{\cosh(Z)} \to 0$ and $\frac{\tanh(Z)}{Z} \to 0$. Taking these order of magnitude argument into account and substituting back into Eq. (A1e) yield

$$\bar{U} \approx Da \times [1 - 0] = \frac{1}{Z^2}. \tag{A2}$$

Setting S = 1 in Eqs. (30) and (32b) reveals the flux ratio for models A and B to be $\gamma|_{\text{Model A}} = \gamma|_{\text{Model B}} = 1$. This indicates that as expected, under fully-filled condition, the heat flux at the porous-fluid interface is the same as the wall heat flux.

Fluid and solid temperatures under model A

Substituting S =1 into Eq. (53) and some re-arrangements result in

$$\Theta_{f2}\Big|_A = \frac{k}{\bar{U}}\left\{\frac{C.(Z^2 - Bi)(1+\gamma+\omega_f+\omega_s)}{Z^2(-\Gamma^2+Z^2)}(\cosh(ZY) - \cosh(Z)) - \frac{C.(Z^2 - Bi)}{Z^2(-\Gamma^2+Z^2)}Z^2\xi - \frac{Bi\,Da}{\Gamma^2}\xi - \right.$$
$$\frac{Bi\left(Da(\omega_f+\omega_s)(1+\gamma+\omega_f+\omega_s) - \bar{U}(\omega_f+\omega_s)\right)}{\Gamma^2}\xi + \frac{DaBi}{\Gamma^2}\frac{1}{2}(Y^2 - 1) + \frac{Bi\left(Da(\omega_f+\omega_s) - \bar{U}(\omega_f+\omega_s)\right)}{\Gamma^2}\left(\frac{Y^2}{2} - \frac{1}{2}\right) - \tag{A3a}$$
$$\left.\bar{U}\xi\omega_f\right\}.$$

Through substituting for C from Eq. (A1c), noting that in the limit of $Da \to 0$, $Z \to \infty$ and $\bar{U} \approx Da$, and after some algebra, it can be shown that

$$\Theta_{f2}\Big|_A = \frac{k}{\bar{U}}\frac{Da.(Z^2-Bi)(1+\gamma+\omega_f+\omega_s)}{Z^2(-\Gamma^2+Z^2)}\left(1-\frac{\cosh(ZY)}{\cosh(Z)}\right) - \left(\frac{k}{\bar{U}}\frac{-Da.(Z^2-Bi)(1+\gamma+\omega_f+\omega_s)}{(-\Gamma^2+Z^2)}\frac{\cosh(Z)}{\cosh(Z)} + \frac{k}{\bar{U}}\frac{Da.Bi}{\Gamma^2} + \frac{k}{\bar{U}}\bar{U}\omega_f\right)\xi + \frac{k}{\bar{U}}\frac{DaBi}{\Gamma^2}\frac{1}{2}(Y^2 - 1) = -\left(-k\left(1+\omega_s+\omega_f\right) + \frac{kBi}{Bi(1+k)} + k\omega_f\right)\frac{1}{Bi(1+k)}\left(\frac{\cosh(\Gamma Y)}{\cosh(\Gamma)} - 1\right) + \frac{kBi}{Bi(1+k)}\frac{1}{2}(Y^2-1), \tag{A3b}$$

which readily reduces to

$$\Theta_{f2}\Big|_A = \frac{k}{1+k}\left\{\frac{1}{2}(Y^2-1) + \left(\frac{k}{1+k}+\omega_s\right)\frac{1}{Bi}\left(\frac{\cosh(\Gamma Y)}{\cosh(\Gamma)} - 1\right)\right\}. \tag{A4}$$

This is the same as the fluid temperature distribution for model A derived by Yang and Vafai [24]. A similar analysis can be conducted on the temperature distribution of the solid phase. First, the value of *S* in Eq. (53) is set to one. This renders the solid phase temperature distribution as

$$\Theta_s\Big|_A = -\frac{k.Bi}{\bar{U}}\left\{\frac{C.\left(1+\omega_s+\omega_f\right)[\cosh(ZY)-\cosh(Z)(1+\xi Z^2)]}{Z^2(-\Gamma^2+Z^2)} - \frac{Da}{\Gamma^2}\left(1+\omega_f+\omega_s\right)\left(-\xi+\frac{Y^2}{2}-\frac{1}{2}\right) + \frac{\left(\omega_s+\omega_f\right)\bar{U}}{\Gamma^2}\left(-\xi+\frac{Y^2}{2}-\frac{1}{2}\right)\right\} + \omega_s\xi. \tag{A5a}$$

Some re-arrangements and expansions lead to

$$\Theta_s\Big|_A = -\frac{k.Bi}{\bar{U}}\frac{C.\left(1+\omega_s+\omega_f\right)\cosh(ZY)}{Z^2(-\Gamma^2+Z^2)} + \frac{k.Bi}{\bar{U}}\frac{C.\left(1+\omega_s+\omega_f\right)\cosh(Z)}{Z^2(-\Gamma^2+Z^2)} + \frac{k.Bi}{\bar{U}}\frac{C.\left(1+\omega_s+\omega_f\right)}{Z^2(-\Gamma^2+Z^2)}Z^2\xi\cosh(Z) + \frac{k.Bi.Da}{\Gamma^2\bar{U}}\left(-\xi+\frac{Y^2}{2}-\frac{1}{2}\right) + \frac{k.Bi.Da}{\Gamma^2\bar{U}}\left(\omega_s+\omega_f\right)\left(\frac{Y^2}{2}-\frac{1}{2}\right) - \frac{k.Bi.\bar{U}}{\Gamma^2\bar{U}}\left(\omega_s+\omega_f\right)\left(\frac{Y^2}{2}-\frac{1}{2}\right) + \omega_s\xi, \tag{A5b}$$

which simplifies to

$$\Theta_s\Big|_A = -\frac{k.Bi}{\bar{U}}\frac{-Da\left(1+\omega_s+\omega_f\right)}{Z^2(-\Gamma^2+Z^2)}\frac{\cosh(ZY)}{\cosh(Z)} + \frac{k.Bi}{\bar{U}}\frac{-Da\left(1+\omega_s+\omega_f\right)}{Z^2(-\Gamma^2+Z^2)}\frac{\cosh(ZY)}{\cosh(Z)} + \frac{k.Bi}{\bar{U}}\frac{-Da\left(1+\omega_s+\omega_f\right)}{Z^2(-\Gamma^2+Z^2)}Z^2\xi\frac{\cosh(ZY)}{\cosh(Z)} + \frac{k.Bi}{\bar{U}}\frac{Da}{\Gamma^2}(-\xi) + \frac{k.Bi}{\bar{U}}\frac{Da}{2\Gamma^2}(Y^2-1) + \omega_s\xi. \tag{A5c}$$

In the limit of $Z \to \infty$ in which $\overline{U} \approx Da$. Hence, Eq. (A5c) reduces to

$$\Theta_s\Big|_A = \frac{k}{1+k}\left[\frac{1}{2}(Y^2-1) + (\frac{1}{1+k} + \omega_s)\frac{1}{Bi}(1 - \frac{\cosh(\Gamma Y)}{\cosh(\Gamma)})\right]. \quad \text{(A6)}$$

Eq. (A6) is the same as solid phase temperature distribution under model A in Refs. [24]. It should be noted that the definition of the thermal conductivity in the current work is the reverse of that employed by Yang and Vafai [24].

Fluid and solid temperatures under model B

Equation (53) gives the solid temperature under model B. Setting S=1 in this equation yields

$$\Theta_s\Big|_B = \frac{\varphi_2}{\Gamma^2}[\cosh(\Gamma Y) - \cosh(\Gamma)] + \frac{Bi.\frac{k}{\overline{U}}Da.(1+\gamma+\omega_s+\omega_f) - Bi.k.(\omega_s+\omega_f)}{2\Gamma^2}(Y^2-1) - \frac{Bi.\frac{k}{\overline{U}}.(1+\gamma+\omega_s+\omega_f)}{Z(Z^2-\Gamma^2)}.C.[\cosh(ZY) - \cosh(Z)], \quad \text{(A7a)}$$

where

$$\varphi_2 = \frac{\Gamma}{\sinh(\Gamma)}\left[1 + \frac{-Bi.k.(2+\omega_f+\omega_s) + Bik(\omega_f+\omega_s)}{Bi(1+k)} + \frac{Bi.k.(2+\omega_f+\omega_s)(-Da)}{Z(Z^2-\Gamma^2)}\frac{\sinh(Z)}{\cosh(Z)}\right]. \quad \text{(A7b)}$$

It was shown earlier that for S=1, γ approaches the value of one, also as $Z \to \infty$, $\frac{\cosh(ZY)}{\cosh(Z)} \to 0$ and $\overline{U} \approx Da$. Thus, Eqs. (A7a) and (A7b) can be rewritten as

$$\Theta_s\Big|_B = \frac{\varphi_2}{\Gamma^2}[\cosh(\Gamma Y) - \cosh(\Gamma)] + \frac{Bi\frac{k}{Da}Da.(2+\omega_s+\omega_f) - Bi.k.(\omega_s+\omega_f)}{2Bi(1+k)}(Y^2-1) - \frac{Bi.\frac{k}{Da}.(2+\omega_s+\omega_f)}{Z(Z^2-\Gamma^2)}.(-Da).\left[\frac{\cosh(ZY)}{\cosh(Z)} - \frac{\cosh(Z)}{\cosh(Z)}\right] \approx \frac{\varphi_2}{Bi(1+k)}[\cosh(\Gamma Y) - \cosh(\Gamma)] + \frac{2BiK}{2Bi(1+k)}(Y^2-1) \quad \text{(A8a)}$$

and

$$\varphi_2 \approx \frac{\Gamma}{\sinh(\Gamma)}\left[1 - \frac{2k}{1+k}\right] = \frac{\Gamma}{\sinh(\Gamma)}\frac{1-k}{1+k}. \quad \text{(A8b)}$$

Hence, the solid phase temperature becomes

$$\Theta_s\Big|_B = \frac{1-k}{\Gamma.\sinh(\Gamma)(1+\mathrm{k})}[\cosh(\Gamma Y) - \cosh(\Gamma)] + \frac{k}{1+k}(Y^2-1), \quad \text{(A9)}$$

which is identical to that derived by Yang and Vafai [22], if the difference in the definition of *k* is taken into account.

Through a similar procedure for φ_1 (as given by Eq. (54b)) it can be shown that

$$\varphi_1 = \frac{\Gamma}{\sinh(\Gamma)}\left[k - \frac{\frac{k}{Da}Da.Bi.(2)}{\Gamma^2} - \frac{\frac{k}{Da}.(1+1).(-Da).(Z^2-Bi)}{Z(Z^2-\Gamma^2)}\frac{\sinh(Z)}{\cosh(Z)}\right] \approx \frac{\Gamma}{\sinh(\Gamma)}k.\left(\frac{1-k}{1+k}\right). \quad \text{(A10)}$$

Substitution of the expressions developed in Eqs. (A8b) and (A10) for φ_2 and φ_1 into the definition of φ_3 given by Eq. (54d) and after some algebra, φ_3 becomes

$$\varphi_3 = \cosh(\Gamma)\left[-\frac{\Gamma}{\Gamma^2\sinh(\Gamma)}k\left(\frac{k-1}{k+1}\right) - \frac{\Gamma}{Bi\sinh(\Gamma)}\frac{1-k}{1+k}\right] + \frac{k.Bi.(2)}{\Gamma^2}\left(\frac{-1}{Bi} - \frac{1}{2}\right) - \frac{\frac{k}{Da}(2+\omega_f+\omega_s)}{Z^4} - \frac{\omega_s}{Bi}. \quad \text{(A11)}$$

Substituting from Eqs. (A10) and (A11) into the expression for the fluid phase temperature under model B, given by Eq. (52), results in

$$\Theta_{f2}\Big|_B = \frac{\cosh(\Gamma Y)}{\Gamma\sinh(\Gamma)}k.\left(\frac{k-1}{k+1}\right) + \frac{k}{k+1}Y^2 + \frac{\cosh(\Gamma)}{\sinh(\Gamma).\Gamma}\left(\frac{k-1}{k+1}\right) - \frac{2k}{1+k}\frac{1}{Bi} - \frac{k}{1+k} - \frac{\omega_s}{Bi}. \quad \text{(A12a)}$$

Some rearrangements reduce this equation to

$$\Theta_{f2}\Big|_B = \frac{k-1}{(k+1)\sinh(\Gamma)}[k\cosh(\Gamma Y) + \cosh(\Gamma)] + \frac{k}{1+k}(Y^2-1) - \frac{2k}{Bi(1+k)} - \frac{\omega_s}{Bi}, \quad \text{(A12b)}$$

which is the same as the solution developed by Yang and Vafai [24] for the distribution of fluid phase temperature under model B.

LTE temperature distribution

Setting *S*=1 in Eq. (58) and noting that $\Theta_{f1}(1) = \Theta_w = 0$

$$\Theta(Y) = \frac{k}{1+k}\left\{\frac{1}{\overline{U}}\left[\frac{-Da}{Z^2}\left(\frac{\cosh(ZY)}{\cosh(Z)} - 1\right) + \frac{1}{2}Da.(Y^2-1)\right](1+\omega_f+S\omega_s) - \frac{1}{2}(\omega_f+\omega_s)(Y^2-1)\right\}. \quad \text{(A13a)}$$

It has been already shown that as as $\to \infty$, $\frac{\cosh(ZY)}{\cosh(Z)} \to 0$ and $\overline{U} \approx Da$. Hence,

$$\Theta(Y) = \frac{k}{2(1+k)}(Y^2 - 1). \tag{A13b}$$

Once corrected for the definition of *k*, this equation becomes identical to that developed in Ref [24]. In the limit of fully filled channel ($S \to 1$), $\Theta_{f1} \to 0$.

Appendix B. Analytical expressions for temperature gradient flux bifurcation

According to Yang and Vafai [24], temperature gradient bifurcation occurs when the sign of Σ becomes negative. This is defined as

$$\Sigma = \frac{\Theta'_{f2}(Y)\big|_{\text{ModelA}}}{\Theta'_{s}(S)\big|_{\text{ModelA}}}. \tag{B1}$$

Differentiating Eq. (42) with respect to Y and evaluating the result at Y=S results in

$$\Theta'_{f2}(S)\big|_{\text{ModelA}} = \tag{B2}$$

$$\frac{k}{\bar{U}}\Bigg\{\frac{C.(Z^2 - Bi)(1+\omega_f + S\omega_s)}{Z^2(-\Gamma^2 + Z^2)}\left(\sinh(ZS) - \frac{Z.\cosh(Z)}{\Gamma}\tanh(\Gamma S)\right) - \frac{Bi\left(Da(1+\omega_f+S\omega_s) - \bar{U}(\omega_f+\omega_s)\right)}{\Gamma^2}\left[\frac{-1}{\Gamma}\tanh(\Gamma S) + S\right] + U_P(S)(1+\omega_f + S\omega_s)\frac{1}{\Gamma}\tanh(\Gamma S) - \bar{U}\omega_f\frac{1}{\Gamma}\tanh(\Gamma S)\Bigg\}$$

Similarly, the following expression is produced by differentiating Eq. (43),

$$\Theta'_{s}(S)\big|_{\text{ModelA}} = -Bi\frac{k}{\bar{U}}\left\{\frac{C(1+S\omega_s+\omega_f)}{Z^2(-\Gamma^2+Z^2)}\left[\sinh(ZS) - \frac{Z.\cosh(ZS)}{\Gamma}\tanh(\Gamma S)\right] + \left[-\frac{Da}{\Gamma^2}(1+S\omega_s+\omega_f) + \frac{(\omega_s+\omega_f)\bar{U}}{\Gamma^2}\right]\left(\frac{-1}{\Gamma}\tanh(\Gamma S) + S\right)\right\} - \frac{\omega_s}{\Gamma}\tanh(\Gamma S). \tag{B3}$$

Nomenclature

a_{sf}	Interfacial area per unit volume of porous media (m^{-1})
A	Parameter defined by Eq. (24)
B	Parameter defined by Eq. (25)
Bi	Biot number, $\frac{a_{sf} h_{sf} h_0^2}{(1-\varepsilon)k_s}$
C	Parameter defined by Eq. (27)
C_p	Specific heat of the fluid, (J $Kg^{-1}K^{-1}$)
Da	Darcy number, K/h_o^2
h_{sf}	Fluid to solid heat transfer coefficient (W $m^{-2}K^{-1}$)
h_0	Height of the channel (m)
h_p	Porous substrate thickness (m)
K	Permeability of the porous medium (m^2)
k	Ratio of solid effective thermal conductivity to that of the fluid, $(1-\varepsilon)k_s/(\varepsilon k_f)$
k_f	Thermal conductivity of the fluid (W $m^{-1}K^{-1}$)
$k_{f,eff}$	Effective thermal conductivity of the fluid, εk_f
k_s	Thermal conductivity of the solid (W $m^{-1}K^{-1}$)
$k_{s,eff}$	Effective thermal conductivity of the solid, $(1-\varepsilon)k_s$
O_1	Constant parameter defined by Eq. (51b)
O_2	Constant parameter defined by Eq. (51c)
q	Heat flux (W m^{-2})
S	Ratio of the porous medium thickness to the channel height, h_p/h_0
S_f	Energy source in fluid phase per unit volume (W/m^3)
S_s	Energy source in solid phase per unit volume (W/m^3)
T	Temperature (K)
u	Longitudinal velocity (m/s)
$\overline{u}$	Average velocity (m/s)
u_r	Characteristic velocity, $-\frac{h_0^2}{\mu}\frac{\partial p}{\partial x}$
U	Dimensionless velocity, u/u_r
$\overline{U}$	Dimensionless average velocity
x	longitudinal coordinate (m)

y	Transverse coordinate (m)
Y	Dimensionless y coordínate, y/h_0
Z	Constant parameter, $\sqrt{1/Da}$

Greek Symbols

γ	Ratio of wall heat flux to the heat flux at the interface, $q_w/q_{\text{interface}}$
Γ	Constant parameter defined by Eq. (54e)
ε	Porosity of the porous medium
Θ	Dimensionless temperature
μ	Viscosity (Kg $m^{-1}s^1$)
ρ	Density, (kg/m^3)
ξ	Constant parameter used in Eq. (43)
$\varphi 1$	Constant parameter defined by Eq. (54b)
$\varphi 2$	Constant parameter defined by Eq. (54c)
$\varphi 3$	Constant parameter defined by Eq. (54d)
ω_f	Normalised energy source term in fluid defined by Eq. 22i
ω_s	Normalised energy source term in fluid defined by Eq. 22j

Subscripts

eff	Effective property
f	Fluid
f_1	Fluid in the open region
f_2	Fluid in the porous medium
p	Porous medium
s	Solid
w	Wall
interface	The interface between the porous medium and the clear region

Superscripts

−	Mean value
´,´´,´´´,´´´´	First, second, third, and forth derivatives with respect to Y

References

[1] Vafai, K., Porous Media: Applications in Biological Systems and Biotechnology, 2011, CRC Press, Boca Raton, FL.

[2] Mahjoob, S. Vafai K., Analytical characterization of heat transport through biological media incorporating hyperthermia treatment, *International Journal of Heat and Mass Transfer* 2009; **52**: 1608–1618.

[3] Kaviany M., Principle of heat transfer in porous media, second ed., 1995, Spring-Verlag, New York.

[4] Ingham, D.B., Pop I., (Eds.), Transport Phenomena in Porous Media III. Elsevier, Oxford, 2005.

[5] Vadasz P., (Ed.), Emerging Topics in Heat and Mass Transfer in Porous Media. Springer, Berlin, 2008.

[6] Nield, D. A., Adrian B., Convection in Porous Media, (4th ed.) 2013, Springer, New York.

[7] Vafai K., Handbook of porous media, 2000, Marcel Dekker, Ohio.

[8] Amiri A., Vafai K., Kuzay T.M., Effects of boundary conditions on non-Darcian heat transfer through porous media and experimental comparisons, *Numerical Heat Transfer Part A*, 1995; **27**, 651–664.

[9] Alazmi, B., Vafai, K. Constant wall heat flux boundary conditions in porous media under local thermal non-equilibrium conditions, *International Journal of Heat and Mass Transfer*, 2002, **45(15)**, 3071-3087.

[10] Yang C., Ando K., Nakayama A., A Local thermal non-equilibrium analysis of fully developed forced convective flow in a tube filled with a porous medium, *Journal of Transport in Porous Media* 2011; **89**, 237–249.

[11] Yang C., Nakayama A., Liu, W., Heat transfer performance assessment for forced convection in a tube partially filled with a porous medium, *International Journal of Thermal Sciences* 2012; **54,** 98-108.

[12] Dixon, A. G., Cresswell, D. L., Theoretical prediction of effective heat transfer parameters in packed beds, *AIChE Journal*, 1979; **25(4),** 663-676.

[13] Sözen, M., Vafai, K., Analysis of the non-thermal equilibrium condensing flow of a gas through a packed bed. *International Journal of Heat and Mass Transfer*, 1990; **33(6),** 1247-261.
[14] Amiri, A., Vafai K., Analysis of dispersion effects and non thermal equilibrium, non Darcian, variable porosity, in compressible flow through porous media, *International Journal of Heat and Mass Transfer* **1994**; 37, 939-954.
[15] Lee, D.Y., Vafai K., Analytical characterization and conceptual assessment of solid and fluid temperature differential in porous media, *International Journal of Heat and Mass Transfer* 1999, **42,** 423-435.
[16] Alazmi B., Vafai K., Analysis of variants within the porous media transport models. *Journal of Heat Transfer*, 2000; **122(2),** 303-326.
[17] Marafie, A., Vafai, K., , Analysis of non-Darcian effects on temperature differentials in porous media, *International Journal of Heat and Mass Transfer* 2001; **44**, 4401-4411.
[18] Kim, S.J., Jang S.P., Effects of the Darcy number, the Prandtl number, and the Reynolds number on local thermal non-equilibrium, *International Journal of Heat and Mass Transfer* 2002; **45**, 3885–3896.
[19] Jeng, T.M., Tzeng, S.C., Hung Y.H., An analytical study of local thermal equilibrium in porous heat sinks using fin theory, *International Journal of Heat and Mass Transfer* 2006; **49,** 1907–1914.
[20] Khashan, S.A. , Al-Nimr, M.A., Validation of the local thermal equilibrium assumption in forced convection of non-Newtonian fluids through porous channels, *Transport in Porous Media*, 2005; **61**, 291–305.
[21] Khashan, S.A., Al-Amiri, A.M., Al-Nimr, M.A., Assessment of the local thermal non-equilibrium condition in developing forced convection flows through fluid-saturated porous tubes, Applied Thermal Engineering 2005; **25,** 1429–1445.
[22] Mahjoob, S., Vafai S., Analytical characterization and production of an isothermal surface for biological and electronic applications, *Journal of Heat Transfer*, 2009, **131**, 052604-1.
[23] Mahjoob, S., Vafai K., Analysis of bioheat transport through a dual layer biological media, *Journal of Heat Transfer*, 2010; **132**, 031101-1.
[24] Yang, K., Vafai, K., Analysis of temperature gradient bifurcation in porous media – an exact solution, *International Journal of Heat Mass Transfer* 2010; **53**, 4316–4325.

[25] Ouyang, X.L., Vafai K., Jiang P.X., Analysis of thermally developing flow in porous media under local thermal non-equilibrium conditions, *International Journal of Heat and Mass Transfer* 2013; **67,** 768–775.
[26] Nimvari, M.E., Maerefat, M., El-Hossaini, M.K., Numerical simulation of turbulent flow and heat transfer in a channel partially filled with a porous media, *International Journal of Thermal Sciences* 2012; **60,** 131-141.
[27] Maerefat, M., Mahmoudi S.Y., Mazaheri, K., Numerical simulation of forced convection enhancement in a pipe by porous inserts, *Heat Transfer Engineering* 2011; **32,** 45-61.
[28] Shokouhmand H., Jam F., Salimpour M.R., The effect of porous insert position on the enhanced heat transfer in partially filled channel, *International Communication in Heat Mass Transfer* 2011; **38,** 1162-1167.
[29] Mohamed A. Teamah, Wael M. El-Maghlany, Mohamed M. Khairat Dawood, Numerical simulation of laminar forced convection in horizontal pipe partially or completely filled with porous material, *International Journal of Thermal Science,* 2011; **50,** 1512–1522.
[30] Cekmer, O., Mobedi M., Ozerdem, B., Pop, I., Fully developed forced convection in a parallel plate channel with a centered porous layer, *Transport in Porous Media,* 2012; **93,** 179–201.
[31] Ucar, E., Mobedi, M., Pop, I., Effect of an inserted porous layer located at a wall of a parallel plate channel on forced convection heat transfer, *Transport in Porous Media,* 2013; **98(1),** 35-57.
[32] Forooghi, P., Abkar, M., Saffar-Avval, M., Steady and unsteady heat transfer in a channel partially filled with porous media under thermal non-equilibrium condition, *Transport Porous Media,* 2011; **86,** 177–198.
[33] Yang, K., Vafai, K., Analysis of heat flux bifurcation inside porous media incorporating inertial and dispersion effects – An exact solution, *International Journal of Heat and Mass Transfer* , 2011; **54,** 5286-5297.
[34] Yang, K., Vafai, K., Restrictions on the validity of the thermal conditions at the porous-fluid interface: an exact solution, *Journal of Heat Transfer,* 2011; **133(11),** 112601.
[35] Mahmoudi, Y., Karimi, N., Numerical investigation of heat transfer enhancement in a pipe partially filled with a porous material under local thermal non-equilibrium condition,

International Journal of Heat Mass Transfer 2014; **68,** 161–173.
[36] Mahmoudi, Y., Maerefat, M., Analytical investigation of heat transfer enhancement in a channel partially filled with a porous material under local thermal non-equilibrium condition, *International Journal of Thermal Sciences* 2011; **50**, 2386-2401.
[37] Mahmoudi, Y., Karimi, N., Mazaheri, K., Analytical investigation of heat transfer enhancement in a channel partially filled with a porous material under local thermal non-equilibrium condition: Effects of different thermal boundary conditions at the porous-fluid interface, *International Journal of Heat and Mass Transfer* 2014; **70**, 875–891.
[38] Karimi, N., Mahmoudi, Y., Mazaheri, K., Temperature fields in a channel partially filled with a porous material under local thermal non-equilibrium condition–An exact solution. *Proceedings of the Institution of Mechanical Engineers, Part C: Journal of Mechanical Engineering Science,* 2014; **228**(15), 2778-2789**.**
[39] Mohamad, A.A., Heat transfer enhancement in heat exchangers fitted with porous media, Part I: constant wall temperature, *International Journal of Thermal Sciences* 2003; **42**, 385-395.
[40] Pavel, B.I., Mohammad, A.A., An experimental and numerical study on heat transfer enhancement for gas heat exchangers fitted with porous media, *International Journal of Heat and Mass Transfer* 2004; **47,** 4939-4952.
[41] Vafai, K.R., Thiyagaraja, R., Analysis of flow and heat transfer at the interface region of a porous medium, *International Journal of Heat and Mass Transfer* 1987; **30,** 1391-1405.
[42] Alazmi, B., Vafai, K., Analysis of fluid flow and heat transfer interfacial conditions between a porous medium and a fluid layer, *International Journal of Heat and Mass Transfer* 2001, **44,** 1735-1749.
[43] Givler, R.C., Altobelli, S.A., A determination of the effective viscosity for the Brinkman–Forchheimer flow model, *Journal of Fluid Mechanics* 1994; **258**, 355–370.
[44] Beavers, G.S., Joseph, D.D., Boundary conditions at a naturally permeable wall, *Journal of Fluid Mechanics* 1967; **30** 197–207.